IS-T-226

AMES LABORATORY

Iowa State University

Ames, Iowa

AEC Contract No. W-7405-eng-82

GENERALIZED SUSCEPTIBILITIES AND MAGNETIC ORDERING OF HEAVY RARE EARTHS

by

William Edwin Evenson

Ph.D. Thesis, May, 1968

DISCLAIMER

GENERALIZED SUSCEPTIBILITIES AND MAGNETIC ORDERING OF HEAVY RARE EARTHS

by

William Edwin Evenson

A Dissertation Submitted to the
Graduate Faculty in Partial Fulfillment of
The Requirements for the Degree of
DOCTOR OF PHILOSOPHY

Major Subject: Physics

Approved:

S. H. Liu
In Charge of Major Work

D. B. Adams
Head of Major Department

J. B. Page
Dean of Graduate College

Iowa State University
Ames, Iowa

May 1968

TABLE OF CONTENTS

GENERALIZED SUSCEPTIBILITIES AND MAGNETIC ORDERING OF HEAVY RARE EARTHS[1]

William Edwin Evenson

Under the supervision of S. H. Liu
From the Department of Physics
Iowa State University

ABSTRACT

Within the framework of Ruderman-Kittel-Kasuya-Yosida indirect-exchange interaction theory, the generalized susceptibilities, $\chi(q)$, have been calculated for the heavy rare-earth metals, Gd, Dy, Er, and Lu, along the line Γ to A of the Brillouin zone. The energy bands used in this calculation were realistic bands obtained by Keeton and Loucks using the relativistic-augmented-plane-wave method. The matrix elements involved in the susceptibilities were taken to be constants so that the susceptibilities calculated here contain only information from the energy bands.

To develop a reliable numerical procedure we examined in detail two sets of energy bands which could be calculated analytically as well as numerically. These bands were chosen to give spherical and cubic Fermi surfaces. The results obtained from them showed us how to eliminate any spurious features in the susceptibilities arising from the numerical

---

[1]USAEC Report IS-T-226. This work was performed under Contract W-7405-eng-82 with the Atomic Energy Commission.

calculation, and once these spurious features were removed these special bands demonstrated that the numerical procedures were quite reliable.

Cubic and spherical Fermi surfaces were chosen because they illustrate two extremes in the features of the susceptibilities: the cubic surface has many points separated by the same wave vector, Q, so there is "nesting" of areas of the Fermi surface for $q = Q$; the spherical surface has only point to point nesting for any particular q. The nesting of areas results in a logarithmic divergence in the susceptibility, whereas the nesting of lines or points results only in a general falling off of the susceptibility. This fact is clearly illustrated in our two special cases. It is also possible to relate the features of the susceptibilities calculated for the rare earths to the geometries of their Fermi surfaces in the same way. We have done this and related the maxima of our calculated susceptibilities to the magnetic ordering periodicity observed experimentally for each of the metals considered. The agreement between theory and experiment was found to be quite satisfactory.

INTRODUCTION

The purpose of this work is to calculate the generalized susceptibilities of the heavy rare earths, gadolinium, dysprosium, erbium, and lutetium, using realistic energy bands in order to show the effect of the Fermi surface on the determination of the magnetic structure of these metals. This calculation will also make a rough check of the energy bands near the Fermi energy by comparing features of the calculated susceptibilities, which are very sensitive to the bands near the Fermi energy, with experimental information.

Calculations of the spatial extent of the charge densities of rare-earth atoms and work on cohesive energies of the rare-earth metals show that the ions in the heavy rare-earth metals do not overlap appreciably with their neighbors. In fact, the ion cores have radii of the order of 0.5 A while nearest neighbor separations in the crystals are about 3 to 4 A. Figure 1 is plotted from the calculations of Herman and Skillman (1963) for the gadolinium atom, and is typical of the spatial extent of the wave functions for the rare earths: the 4f-shell is highly localized, while the 6s-electrons are smeared through the crystal. The dotted line shows approximately how the 6s wave function is flattened out in the metal.

An important question to be raised by the absence of a significant amount of overlap between ions was how can these metals form periodic moment arrangements, ferromagnetism and

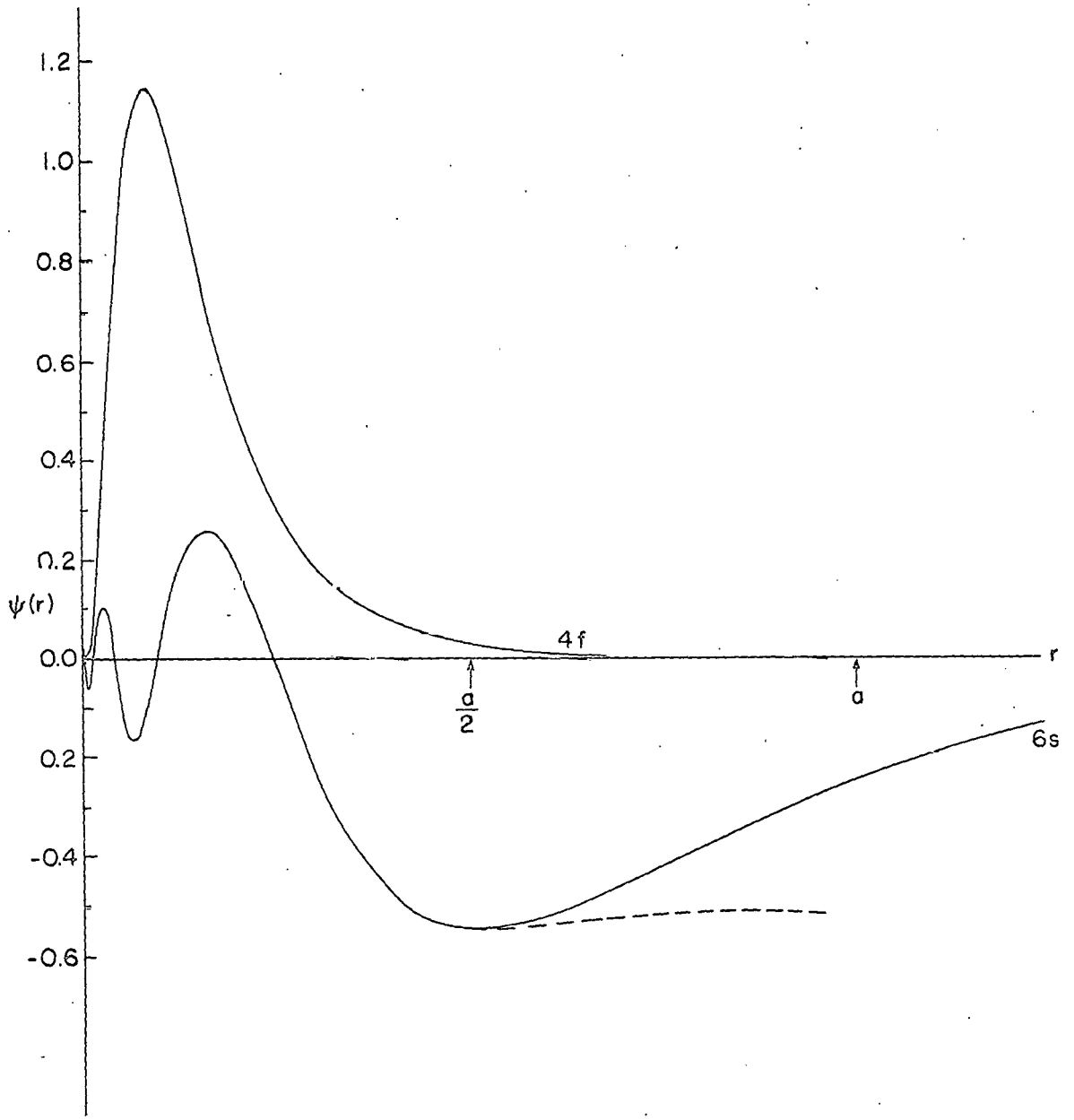

Figure 1. Atomic wave functions for Gd. The dashed line approximates the 6s wave function for Gd metal

various kinds of antiferromagnetism, if the ions do not overlap to "tell" each other how each moment is pointing? If there is no overlap, how does an ionic moment "know" where its neighbors are pointing? The answer to this question lies in the ideas of "indirect exchange," in which the conduction electrons are visualized as passing the necessary information for the lining up of the moments from a given ion to the others.

The first important analysis of the indirect-exchange interaction was done by Ruderman and Kittel (1954) with direct application to the case of nuclei interacting via the hyperfine interaction with the conduction electrons. In later important papers Kasuya (1956) and Yosida (1957) applied the ideas of indirect exchange to magnetic materials and developed what has come to be known as the Ruderman-Kittel-Kasuya-Yosida (hereafter RKKY) interaction model for metals such as the rare earths where the ions have no direct overlap to convey magnetic ordering information from one to another. (See also Liu 1961b) The results of these theories gave an interaction which depends on 1) the exchange integrals between the localized ionic cores with their large moments and the conduction-electron wave functions at the ion sites, and 2) the energy bands of the conduction electrons and their Fermi surface. The energy bands of these materials have not been well-known, so the standard procedure has been to insert free-electron

bands in the evaluation of the interaction. Another approximation that has been made in the evaluation of the indirect-exchange interaction is to put the exchange integrals (matrix elements) to be constant, or at best functions of $|\underline{k}'-\underline{k}|$ only. Still a third point where important approximations have been made is in the basic assumption at the outset that the charge clouds are spherically symmetric to a good approximation so that the Heisenberg $\underline{S}\cdot\underline{s}$ type of interaction Hamiltonian is valid. This is not precisely true in the case of the rare earths because of the orbital contribution to the magnetic moment, as pointed out by Elliott and Thorpe (1968). The asymmetry and finite size of the charge clouds also affect the form of the exchange integrals, and hence the approximation that they are independent of $\underline{k}$ and $\underline{k}'$ (Liu 1961a, Specht 1967, and Kaplan and Lyons 1963).

Kubo (1957) has done important work on analyzing the response of a system to a stimulus in the approximation of linear response. Applied to magnetic systems, this theory gives a generalized susceptibility, $\chi(\underline{q})$, which is the response of the magnetization of the electron gas in the metal to a spatially-varying field characterized by wave vector $\underline{q}$. It turns out that this generalized susceptibility has the same form as the Fourier transform of the RKKY interaction, but with somewhat different matrix elements; therefore, they differ only by a constant factor in the approximation that the matrix

elements are constant and independent of $\underline{k}$ and $\underline{k}'$. Hence, the generalized susceptibility can be related to the magnetic interaction energy of the system. It is proportional to the negative of the magnetic energy, so the maximum in the susceptibility will determine the minimum of the energy and hence the stable wave vector $\underline{Q}$ which characterizes the magnetic ordering. So if the stable magnetic structure in the region of interest is helical, the wave vector $\underline{Q}$ at the maximum in the susceptibility should be just the right size and direction to reflect the periodicity of the helix.

The present work takes advantage of the recent availability of more realistic energy bands for the conduction electrons in the heavy rare earths (Keeton and Loucks 1968) to consider the generalized susceptibility and the RKKY interaction beyond the free-electron assumption. The other approximations have remained; we have treated the exchange integral as though it were independent of $\underline{k}$ and $\underline{k}'$, and we have not considered the effects of a finite or asymmetric charge cloud. Because of the negligible overlap between ions, however, we felt that the worst of the approximations was the use of free-electron bands, the other approximations not being quite as important. The results of this work seem to bear out our contention to some extent since we find ordering arrangements for the heavy rare earths in reasonably good agreement with experiment.

The use of paramagnetic energy bands in the calculation of χ limits our conclusions to what is happening very close to the highest ordering temperature for the particular metal in question because we assume that the magnetic interactions are small and perturb the bands only weakly. Statistical mechanical treatment of spin correlations shows that thermal fluctuations destroy any net long-range order in the spin system at a critical temperature. If we consider an effective field approximation to the magnetic interaction, following the treatment of Villain (1959), where the effective field at a lattice point is proportional to the net magnetization at that point, then we see that thermal fluctuations make the net magnetization, and hence the effective field, small near the critical temperature. Therefore, when we are near the critical temperature, the magnetic interaction perturbs the paramagnetic bands very weakly, so our perturbation calculation of χ using paramagnetic bands should be valid. Away from the critical temperature, however, the magnetic interactions become strong, and the paramagnetic bands are no longer the correct ones to use in calculating $\chi(\underline{q})$.

Lomer (1962) was the first to point out the connection between the Fermi surface and the magnetic ordering of metals. Using realistic energy bands to calculate the indirect-exchange interaction allows us to check this idea quantitatively in heavy rare earths. It is particularly interesting to observe the trends in the Fermi surfaces along side of the trends in

the susceptibilities through the whole series of heavy rare earths (gadolinium to lutetium). We have studied four of the metals, Gd, Dy, Er, and Lu, which should be quite representative of the whole series. It will also be of interest in the future when the energy bands of the other metals become available to fill in the gaps.

THE INDIRECT-EXCHANGE INTERACTION

The Ruderman-Kittel-Kasuya-Yosida Interaction

We can briefly summarize the physical ideas involved in the indirect-exchange interaction model developed by Ruderman, Kittel, Kasuya, and Yosida as follows: In cases of low concentration magnetic impurities or in the rare-earth metals, i.e. cases where magnetic ion cores are sufficiently small or far apart that there is essentially no overlap, the unfilled d- or f-shells retain some of their Hund's Rule magnetization in the solid. By an exchange interaction with the s-band conduction electrons the d- or f-shell moments polarize the spins of the conduction electrons in the neighborhood of the ion. The conduction electrons, constrained by the Pauli exclusion principle, respond with characteristic wavelength $\lambda_F = 2\pi/k_F$, and the resulting spin polarization is oscillatory and long-ranged. The other magnetic atoms then undergo ferromagnetic or antiferromagnetic interactions with the one in question depending on whether they are in a trough or on a crest of the polarization wave. The magnitude of the interaction gradually decreases with distance. In a crystal where there are many magnetic atoms, such as a rare-earth metal, it is very difficult to determine the net relative spin orientation between neighboring ions because this is determined by the superposition at that ion site of the polarization waves in the conduction electrons due to all the other ions in the crystal. Therefore

we must look at the interaction in quite a lot of detail to predict the ordering arrangement in a given material.

An excellent survey of the Ruderman-Kittel-Kasuya-Yosida indirect-exchange interaction in magnetic metals is found in Mattis (1965). We will look at the derivation of that interaction in this section from about the same point of view as Mattis, but including points of special interest to the present calculation. The approach is to assume the existence of an effective Hamiltonian for the metal in question and to apply the exchange interaction between the ionic moments and the conduction electrons at the ion sites as a perturbation. The easiest way to see the form of the interaction is to consider a pair of magnetic solute atoms at points $\underline{R}_1$ and $\underline{R}_2$ in some ideal, nonmagnetic metal characterized by an s-band effective Hamiltonian. We will call the moments "spins" for simplicity even though they are made up of both orbital and spin contributions. Internal Hund's Rule coupling maintains S_1 and S_2, but their relative orientation is determined by coupling through the conduction electrons. Exchange coupling of the localized electrons (f-electrons in our case) with the conduction electrons (s-electrons) is the perturbation:

$$H' = -J[\underline{S}_1 \cdot \underline{s}_c(\underline{R}_1) + \underline{S}_2 \cdot \underline{s}_c(\underline{R}_2)], \qquad (1)$$

where J is the exchange integral between the ions and the s-electrons and the $\underline{s}_c(\underline{R}_i)$ are conduction band spin operators which are defined in the second quantization language as follows:

$$s_c^z = \tfrac{1}{2}(N_{c+} - N_{c-}),$$
$$s_c^+ = c_{c+}^* c_{c-},$$
$$s_c^- = c_{c-}^* c_{c+}, \qquad (2)$$

and $$N_{cm} = c_{cm}^* c_{cm}.$$

The c_{cm}^* and c_{cm} are the usual creation and destruction operators for electrons in the conduction band with spin $+\frac{1}{2}$ or $-\frac{1}{2}$ as m = + or -.

Now we can put the spin operators in the Bloch representation for the case where there are several conduction bands so that

$$s_c^z(\underline{R}_i) = \frac{1}{2N} \sum_{\underline{k},\underline{k}'} \sum_{n,n'} e^{i(\underline{k}-\underline{k}')\cdot\underline{R}_i} (c_{\underline{k}'n'+}^* c_{\underline{k}n+} - c_{\underline{k}'n'-}^* c_{\underline{k}n-}),$$

$$s_c^{\pm}(\underline{R}_i) = \frac{1}{N} \sum_{\underline{k},\underline{k}'} \sum_{n,n'} e^{i(\underline{k}-\underline{k}')\cdot\underline{R}_i} c_{\underline{k}'n'\pm}^* c_{\underline{k}n\mp}, \qquad (3)$$

where n and n' are band indices. Then we rewrite H' as

$$H' = -J \sum_{i=1}^{2} \left\{ s_c^z(\underline{R}_i) S_i^z + \tfrac{1}{2}[s_c^+(\underline{R}_i) S_i^- + s_i^-(\underline{R}_i) S_i^+] \right\}. \qquad (4)$$

We can now calculate the eigenfunctions and eigenvalues for the system in the conduction electron ground state by ordinary perturbation theory on the s-electron part of the total Hamiltonian:

$$H = H_o + H' = \sum_{\underline{k}mn} E_n(\underline{k}) N_{\underline{k}nm} + H', \qquad (5)$$

using H' as in Equation 4. So we obtain in the Bloch representation:

$$H = \sum_{\underline{k}mn} E_n(\underline{k}) N_{\underline{k}nm} - \frac{1}{2N} \sum_{i=1}^{2} \sum_{\underline{k}\underline{k}'} \sum_{nn'} I_{nn'}(\underline{k},\underline{k}')[S_i^z e^{i(\underline{k}-\underline{k}')\cdot\underline{R}_i}$$

$$(C^*_{\underline{k}'n'+} C_{\underline{k}n+} - C^*_{\underline{k}'n'-} C_{\underline{k}n-}) + S_i^- e^{i(\underline{k}-\underline{k}')\cdot\underline{R}_i} C^*_{\underline{k}'n'+} C_{\underline{k}n-} +$$

$$S_i^+ e^{i(\underline{k}-\underline{k}')\cdot\underline{R}_i} c^*_{\underline{k}'n'-} c_{\underline{k}n+}]. \qquad (6)$$

Now H_o does not distinguish between relative spin orientations for the magnetic ions, so it gives a $(2S_1+1)x(2S_2+1) = r$-fold degeneracy of states of the relative orientations of the two solute spins. What we want to see is how H' affects this degeneracy and hence stabilizes some particular relative orientation of the solute spins.

We will call our starting wave functions $|Ft)$, indicating the conduction electrons in the unpolarized Fermi sea ground state, $|F)$, and the two solute spins in a relative state $|t)$ where $t = 1,2,\ldots,r$.

The first-order perturbation to the energy is zero:

$$E_t^{(1)} = (tF|H'|Ft) = 0,$$

since this is just an average over the entire Fermi sea which has no long-range polarization.

We now look at the second-order perturbation to the energy which is of the form:

$$E_t^{(2)} = \sum_{CB,t'}{}' \frac{|(t'CB|H'|Ft)|^2}{E(F.sea) - E(C.B.)} \qquad (7)$$

where $|CB)$ are conduction band states and $|F)$ is the Fermi sea ground state.

The conduction band operators, $c^*_{\underline{k}'n'}$ and $c_{\underline{k}n}$, create elementary excitations with energy $E_{n'}(\underline{k}') - E_n(\underline{k})$. Their matrix elements are unity if $E_n(\underline{k}) < E_F$ and $E_{n'}(\underline{k}') > E_F$, and zero otherwise. So we can put

$$\frac{1}{E(F.sea) - E(C.B.)} = \frac{f_{\underline{k}n}(1 - f_{\underline{k}'n'})}{E_n(\underline{k}) - E_{n'}(\underline{k}')}, \tag{8}$$

where the $f_{\underline{k}n}$ are the Fermi-Dirac distribution functions put in to limit the excitations to the coupling of unoccupied to occupied states. The conduction band states are of the form

$$|CB) = c^*_{\underline{k}_1 n_1 m_1} c_{\underline{k}_2 n_2 m_2} |F), \tag{9}$$

where the single-particle states $\underline{k}_1 n_1$ and $\underline{k}_2 n_2$ are also subject to Fermi-Dirac functions like those of Equation 8, i.e. conduction band states are just like the Fermi sea, but one state below the Fermi energy has been vacated while a state above the Fermi energy has been occupied. We put these states into the matrix elements of Equation 7 and evaluate them as follows:

$$(t'CB|H'|Ft) = -\frac{1}{2N} \sum_i \sum_{\underline{k}\underline{k}'} \sum_{nn'} I_{nn'}(\underline{k},\underline{k}') e^{i(\underline{k}-\underline{k}')\cdot\underline{R}_i}$$

$$\{(t'|S_i^z|t)[(F|c^*_{\underline{k}_1 n_1 m_1} c_{\underline{k}_2 n_2 m_2} c^*_{\underline{k}'n'+} c_{\underline{k}n+}|F)$$

$$- (F|c^*_{\underline{k}_1 n_1 m_1} c_{\underline{k}_2 n_2 m_2} c^*_{\underline{k}'n'-} c_{\underline{k}n-}|F)] + (t'|S_i^+|t)(F|c^*_{\underline{k}_1 n_1 m_1}$$

$$c_{\underline{k}_2 n_2 m_2} c^*_{\underline{k}'n'-} c_{\underline{k}n+}|F) + (t'|S_i^-|t)(F|c^*_{\underline{k}_1 n_1 m_1} c_{\underline{k}_2 n_2 m_2}$$

$$c^*_{\underline{k}'n'+} c_{\underline{k}n-}|F)\}. \tag{10}$$

Now,

$$(F|c^*_{\underline{k}_1 n_1 m_1} c_{\underline{k}_2 n_2 m_2} c^*_{\underline{k}' n' m'} c_{\underline{k} n m}|F) = \delta_{\underline{k}',\underline{k}_2}\delta_{n',n_2}\delta_{m',m_2}$$
$$\delta_{\underline{k},\underline{k}_1}\delta_{n,n_1}\delta_{m,m_1} f_{\underline{k}n}(1-f_{\underline{k}'n'}). \qquad (11)$$

We put this into Equation 10, dropping the Fermi functions which are already contained in Equation 8, and obtain

$$(t'CB|H'|Ft) = -\frac{1}{2N}\sum_i I_{n_1 n_2}(\underline{k}_1,\underline{k}_2) e^{i(\underline{k}_1-\underline{k}_2)\cdot\underline{R}_i}$$
$$(t'|S_i^z(\delta_{m_2,+}\delta_{m_1,+} - \delta_{m_2,-}\delta_{m_1,-}) + S_i^+\delta_{m_2,-}\delta_{m_1,+}$$
$$+ S_i^-\delta_{m_2,+}\delta_{m_1,-}|t). \qquad (12)$$

Now we will replace $\underline{k}_1$ by $\underline{k}$ and $\underline{k}_2$ by $\underline{k}'$ and similarly for n and m for simplicity of notation. Putting Equations 8 and 12 into Equation 7, we have

$$E_t^{(2)} = -\sum_{\underline{k}\underline{k}'}\sum_{nn'}\sum_{mm'}\sum_{t'} \frac{f_{kn}(1-f_{\underline{k}'n'})}{E_{n'}(\underline{k}') - E_n(\underline{k})} \frac{1}{4N^2} I^2_{nn'}(\underline{k},\underline{k}')$$
$$\sum_{ij} e^{i(\underline{k}-\underline{k}')\cdot(\underline{R}_i-\underline{R}_j)} (t'|S_i^z(\delta_{m',+}\delta_{m,+} - \delta_{m',-}\delta_{m,-})$$
$$+ S_i^+\delta_{m',-}\delta_{m,+} + S_i^-\delta_{m',+}\delta_{m,-}|t)(t|S_j^z(\delta_{m',+}\delta_{m,+}$$
$$- \delta_{m',-}\delta_{m,-}) + S_j^-\delta_{m',-}\delta_{m,+} + S_j^+\delta_{m',+}\delta_{m,-}|t'). \qquad (13)$$

Use closure on the states $|t')$ to perform the t' sum and then look at the sums on m and m':

$$E_t^{(2)} = -\frac{1}{4N^2} \sum_{\underline{k}\underline{k}'} \sum_{nn'} \sum_{ij} I^2_{nn'}(\underline{k},\underline{k}') \frac{f_{\underline{k}n}(1-f_{\underline{k}'n'})}{E_{n'}(\underline{k}')-E_n(\underline{k})} e^{i(\underline{k}-\underline{k}')\cdot(\underline{R}_i-\underline{R}_j)}$$

$$\sum_{mm'} (t|[S_j^z(\delta_{m',+}\delta_{m,+} - \delta_{m',-}\delta_{m,-}) + S_j^+\delta_{m',+}\delta_{m,-}$$

$$+ S_j^-\delta_{m',-}\delta_{m,+}][S_i^z(\delta_{m',+}\delta_{m,+} - \delta_{m',-}\delta_{m,-})$$

$$+ S_i^+\delta_{m',-}\delta_{m,+} + S_i^-\delta_{m',+}\delta_{m,-}]|t). \qquad (14)$$

Performing the sums on m and m' in Equation 14, we obtain

$$\sum_{mm'} (t|[\ ]\cdot[\ ]|t) = (t|2S_j^zS_i^z + S_j^+S_i^- + S_i^+S_j^-|t)$$

$$= 2(t|\underline{S}_j\cdot\underline{S}_i|t). \qquad (15)$$

So

$$E_t^{(2)} = -\frac{1}{2N^2} \sum_{ij} \sum_{\underline{k}\underline{k}'} \sum_{nn'} I^2_{nn'}(\underline{k},\underline{k}') \frac{f_{\underline{k}n}(1-f_{\underline{k}'n'})}{E_{n'}(\underline{k}')-E_n(\underline{k})} e^{i(\underline{k}-\underline{k}')\cdot(\underline{R}_i-\underline{R}_j)}$$

$$(t|\underline{S}_i\cdot\underline{S}_j|t). \qquad (16)$$

Equation 16 contains a self-energy term when i = j. This term is independent of relative spin orientations, so it is irrelevant to our problem. We will ignore it and replace $\frac{1}{2}\sum_{ij}$ by $\sum_{(i,j)}$ where (i,j) refers to all possible pairs of spins. Also, we are only looking at two solute atoms to begin with, so i and j can only be 1 or 2. Therefore,

$$E_t^{(2)} = -\frac{1}{N^2} \sum_{\underline{k}\underline{k}'} \sum_{nn'} I^2_{nn'}(\underline{k},\underline{k}') \frac{f_{\underline{k}n}(1-f_{\underline{k}'n'})}{E_{n'}(\underline{k}')-E_n(\underline{k})} e^{i(\underline{k}-\underline{k}')\cdot\underline{R}_{12}}$$

$$(t|\underline{S}_1\cdot\underline{S}_2|t). \qquad (17)$$

But Equation 17 just gives the eigenvalues of the Hamiltonian

$$H_{I.E.} = -J(\underline{R}_{12})\underline{S}_1\cdot\underline{S}_2 \qquad (18)$$

where

$$J(\underline{R}_{ij}) = \frac{1}{N^2} \sum_{\underline{k}\underline{k}'} \sum_{nn'} \frac{I^2_{nn'}(\underline{k},\underline{k}')\, e^{i(\underline{k}-\underline{k}')\cdot\underline{R}_{ij}}\, f_{\underline{k}n}(1-f_{\underline{k}'n'})}{E_{n'}(\underline{k}') - E_n(\underline{k})}. \quad (19)$$

It should now be clear that the straightforward extension of this result to N_M magnetic atoms will just give

$$H_{I.E.} = - \sum_{(i,j)} J(\underline{R}_{ij}) \underline{S}_i \cdot \underline{S}_j, \quad (20)$$

with $J(\underline{R}_{ij})$ as before. We note, however, that this extension is strictly valid only if we treat the ions as points (Elliott and Thorpe 1968), but this is the approximation made throughout the present work.

When we put free-electron energy bands into Equation 19, we obtain the expression often referred to as the Ruderman-Kittel interaction. This result is

$$J(\underline{R}_{ij})_{R.K.} = \frac{J^2}{E_F} \frac{16}{\pi^3} \left(\frac{k_F a_o}{2}\right)^6 \cdot \frac{(\sin 2k_F R_{ij} - 2k_F R_{ij} \cos 2k_F R_{ij})}{(2k_F R_{ij})^4}, \quad (21)$$

where $I_{nn'}(\underline{k},\underline{k}')$ has been taken out as a constant, J, k_F is the Fermi wave vector, and a_o^3 is the volume of the unit cell. Equation 21 can be corrected for finite electronic mean free path, λ, by the inclusion of a factor $e^{-R_{ij}/\lambda}$.

If there is more than one atom in the basis of the unit cell, we have to consider spin operators at each atomic site, so the operators of Equation 3 become

$$s^z_c(\underline{R}_{ir}) = \frac{1}{2N} \sum_{\underline{k}\underline{k}'} \sum_{nn'} e^{i(\underline{k}-\underline{k}')\cdot\underline{R}_{ir}} (c^*_{\underline{k}'n'+} c_{\underline{k}n+} - c^*_{\underline{k}'n'-} c_{\underline{k}n-}),$$

$$s^{\pm}_c(\underline{R}_{ir}) = \frac{1}{N} \sum_{\underline{k}\underline{k}'} \sum_{nn'} e^{i(\underline{k}-\underline{k}')\cdot\underline{R}_{ir}}\, c^*_{\underline{k}'n'\pm} c_{\underline{k}n\mp}, \quad (22)$$

where r is the basis index. The derivation carries through just as before, but a basis index is included everyplace there is a cell index.

We will now consider the Fourier transform of the indirect-exchange interaction, and in the next section of this chapter we will show how it is related to the spin-wave spectrum.

$$F(\underline{q}) \equiv \sum_j J(\underline{R}_j) e^{i\underline{q}\cdot\underline{R}_j}$$

$$= \frac{1}{N^2} \sum_j \sum_{\underline{k}\underline{k}'} \sum_{nn'} I^2_{nn'}(\underline{k},\underline{k}') \frac{e^{i(\underline{k}-\underline{k}')\cdot\underline{R}_j} f_{\underline{k}n}(1-f_{\underline{k}'n'})}{E_{n'}(\underline{k}')-E_n(\underline{k})} e^{i\underline{q}\cdot\underline{R}_j}$$

$$= \frac{1}{N^2} \sum_{\underline{k}\underline{k}'} \sum_{nn'} I^2_{nn'}(\underline{k},\underline{k}') \frac{f_{\underline{k}n}(1-f_{\underline{k}'n'})}{E_{n'}(\underline{k}')-E_n(\underline{k})} \sum_j e^{i(\underline{k}-\underline{k}'+\underline{q})\cdot\underline{R}_j}. \tag{23}$$

But

$$\sum_j e^{i(\underline{k}-\underline{k}'+\underline{q})\cdot\underline{R}_j} = N\delta(\underline{k}+\underline{q}+\underline{K}_o-\underline{k}'),$$

where $\underline{K}_o$ is the reciprocal lattice vector necessary to reduce $\underline{k}+\underline{q}+\underline{K}_o$ to the first Brillouin zone like $\underline{k}'$. Then

$$F(q) = \frac{1}{N} \sum_{\underline{k}} \sum_{nn'} I^2_{nn'}(\underline{k},\underline{k}+\underline{q}+\underline{K}_o) \frac{f_{\underline{k}n}(1-f_{\underline{k}+\underline{q}+\underline{K}_o n'})}{E_{n'}(\underline{k}+\underline{q}+\underline{K}_o)-E_n(\underline{k})}. \tag{24}$$

When we have more than one atom in the basis, we obtain other terms like $F(\underline{q})$ as shown in Equation 24 but corresponding to lattice sums connecting inequivalent atoms from one cell to the next. If we define $\underline{\delta}_r$ as the basis vector from the lattice site in a given cell to the r^{th} atom in the basis in that cell, reference to Equations 19 and 22 allows us to define

$$F_r(\underline{q}) \equiv \sum_j J(\underline{R}_j+\underline{\delta}_r) e^{i\underline{q}\cdot(\underline{R}_j+\underline{\delta}_r)}. \tag{25}$$

$$F_r(\underline{q}) = \frac{1}{N^2} \sum_j \sum_{\underline{k},\underline{k}'} \sum_{nn'} I^2_{nn'}(\underline{k},\underline{k}') \frac{e^{i(\underline{k}-\underline{k}')\cdot(\underline{R}_j+\underline{\delta}_r)} f_{\underline{k}n}(1-f_{\underline{k}'n'})}{E_{n'}(\underline{k}')-E_n(\underline{k})}$$

$$e^{i\underline{q}\cdot(\underline{R}_j+\underline{\delta}_r)}$$

$$= \frac{1}{N^2} \sum_{\underline{k}\underline{k}'} \sum_{nn'} I^2_{nn'}(\underline{k},\underline{k}') \frac{f_{\underline{k}n}(1-f_{\underline{k}'n'})}{E_{n'}(\underline{k}')-E_n(\underline{k})} \sum_j e^{i(\underline{k}-\underline{k}'+\underline{q})\cdot(\underline{R}_j+\underline{\delta}_r)}.$$

So $F_r(\underline{q})$ has an extra factor $e^{i(\underline{k}-\underline{k}'+\underline{q})\cdot\underline{\delta}r} \rightarrow e^{-i\underline{K}_o\cdot\underline{\delta}r}$, a structure factor dependent on the nature of the basis in the unit cell. We write, then,

$$F_r(\underline{q}) = \frac{1}{N} \sum_{\underline{k}} \sum_{nn'} I^2_{nn'}(\underline{k},\underline{k}+\underline{q}+\underline{K}_o) \frac{f_{\underline{k}n}(1-f_{\underline{k}+\underline{q}+\underline{K}_o n'})}{E_{n'}(\underline{k}+\underline{q}+\underline{K}_o)-E_n(\underline{k})} e^{-i\underline{K}_o\cdot\underline{\delta}r}. \quad (26)$$

As we mentioned earlier, we will make the approximation of point ions so that $I^2_{nn'}(\underline{k},\underline{k}') \cong I^2$, a constant that can be taken out of the sums in Equations 19, 24, and 26.

Ferromagnetic Spin Waves and Their Energy Spectrum

Ferromagnetic spin waves consist physically of a precession of each spin about its z-axis, sweeping out a cone in time $2\pi/\omega(\underline{q})$. The radius of the cone is the amplitude, A, of the spin wave, and actually $\omega(\underline{q}) = \omega(\underline{q},A)$, but the amplitude dependence of the spin-wave frequencies is negligible for small-amplitude spin waves. The phase difference between nearest neighbors separated by a distance a is $\varphi = qa$. In the small-amplitude approximation we can find the spin-wave frequencies in the case where the Hamiltonian for the magnetic excitations is the indirect-exchange Hamiltonian of Equations

19 and 20. The quantized spin waves are called "magnons", and they will be the excitations of the diagonalized Hamiltonian,

$$H = \sum_{(i,j)} J_{ij} \underline{S}_i \cdot \underline{S}_j = \sum_{\underline{k}} \omega(\underline{k}) b^*_{\underline{k}} b_{\underline{k}} + \text{constants}, \tag{27}$$

where $b^*_{\underline{k}}$ and $b_{\underline{k}}$ are magnon creation and annihilation operators. We proceed as follows:

Constants of the motion of H include total spin, $\mathcal{S}^2 = (\sum_j \underline{S}_j)^2$, and the z-component, $\mathcal{S}_z = \sum_j S^z_j$.

$$\begin{aligned} \mathcal{S}^2 |0) &= NS(NS+1)|0), \\ \mathcal{S}_z |0) &= NS|0), \end{aligned} \tag{28}$$

where N is the total number of spins and they are all lined up ferromagnetically in the ground state.

We also note that S_x, S_y, and S_z are not independent but are connected by $\underline{S}\cdot\underline{S} = S(S+1)$, quantum mechanically. To go to independent operators, we use the Holstein-Primakoff transformation (Holstein and Primakoff 1940):

$$\begin{aligned} S^+_j &= \sqrt{2S}\left[1 - \frac{a^*_j a_j}{2S}\right]^{\frac{1}{2}} a_j, \\ S^-_j &= \sqrt{2S}\, a^*_j \left[1 - \frac{a^*_j a_j}{2S}\right]^{\frac{1}{2}} \\ S^z_j &= S - a^*_j a_j. \end{aligned} \tag{29}$$

Holstein and Primakoff showed that the a* and a were boson operators satisfying the commutation relations

$$\begin{aligned} [a_i, a^*_j] &= \delta_{ij}, \\ [a_i, a_j] &= [a^*_i, a^*_j] = 0. \end{aligned} \tag{30}$$

It can also be shown (Mattis 1965, for example) that the a* and a of the Holstein-Primakoff representation are very closely related to Schwinger's harmonic oscillator operators in his coupled-boson representation (Schwinger 1952). In the Bloch picture we get

$$b_{\underline{k}} = \frac{1}{\sqrt{N}} \sum_j e^{i\underline{k}\cdot\underline{R}_j} a_j,$$

$$[b_{\underline{k}}, b^*_{\underline{k}'}] = \delta_{\underline{k},\underline{k}'}, \tag{31}$$

$$[b_{\underline{k}}, b_{\underline{k}'}] = [b^*_{\underline{k}}, b^*_{\underline{k}'}] = 0.$$

Now, we are considering small-amplitude spin waves, so there is not much spin reversal, and we can expand the square roots in Equations 29 to lowest order in the $b_{\underline{k}}$:

$$S^+_j = \sqrt{\frac{2S}{N}} \sum_{\underline{k}} e^{-i\underline{k}\cdot\underline{R}_j} b_{\underline{k}} + O(b^2),$$

$$S^-_j = \sqrt{\frac{2S}{N}} \sum_{\underline{k}} e^{i\underline{k}\cdot\underline{R}_j} b^*_{\underline{k}} + O(b^2), \tag{32}$$

$$S^z_j = S - \frac{1}{N} \sum_{\underline{k}\,\underline{k}'} e^{i(\underline{k}-\underline{k}')\cdot\underline{R}_j} b^*_{\underline{k}} b_{\underline{k}'}.$$

But $\mathcal{S}_z = \sum_j S^z_j$, so

$$\mathcal{S}_z = NS - \sum_{\underline{k}} b^*_{\underline{k}} b_{\underline{k}}. \tag{33}$$

$\mathcal{S}_z$ can only have the values NS,NS-1,NS-2,...., as is clear from Equation 28. Therefore, $b^*_{\underline{k}} b_{\underline{k}}$ must be an integral occupation number operator for a state $\underline{k}$. The $b^*_{\underline{k}}$ and $b_{\underline{k}}$ are creation and annihilation operators for elementary excitations characterized by a wave-vector $\underline{k}$, and a frequency $\omega(\underline{k})$. These

elementary excitations are spin waves or magnons, and the $b_{\underline{k}}$ are the magnon operators of Equation 27.

We can write H in magnon variables as

$$H = -\sum_{(i,j)} J_{ij}[(S - \frac{1}{N}\sum_{\underline{k}\underline{k}'} e^{i(\underline{k}-\underline{k}')\cdot\underline{R}_i} b^*_{\underline{k}} b_{\underline{k}'})(S - \frac{1}{N}\sum_{\underline{k}\underline{k}'} e^{i(\underline{k}-\underline{k}')\cdot\underline{R}_j} b^*_{\underline{k}} b_{\underline{k}'})$$

$$+ \frac{S}{N}\sum_{\underline{k}\underline{k}'}(e^{-i\underline{k}\cdot\underline{R}_i} e^{i\underline{k}'\cdot\underline{R}_j} b_{\underline{k}} b^*_{\underline{k}'} + e^{i\underline{k}\cdot\underline{R}_i} e^{-i\underline{k}'\cdot\underline{R}_j} b^*_{\underline{k}} b_{\underline{k}'})]$$

$$= -\sum_{(i,j)} J_{ij}[S^2 - \frac{S}{N}\sum_{\underline{k}\underline{k}'}(e^{i(\underline{k}-\underline{k}')\cdot\underline{R}_i} b^*_{\underline{k}} b_{\underline{k}'} + e^{i(\underline{k}-\underline{k}')\cdot\underline{R}_j} b^*_{\underline{k}} b_{\underline{k}'}$$

$$- e^{-i\underline{k}\cdot\underline{R}_i} e^{i\underline{k}'\cdot\underline{R}_j} b_{\underline{k}} b^*_{\underline{k}'} - e^{i\underline{k}\cdot\underline{R}_i} e^{-i\underline{k}'\cdot\underline{R}_j} b^*_{\underline{k}} b_{\underline{k}'})] \qquad (34)$$

The first term is just a constant term, $-\sum_{(i,j)} J_{ij} S^2$, and we will drop it for the time being. Then

$$H = \frac{S}{N}\sum_{(i,j)} J_{ij}[\sum_{\underline{k},\underline{k}'}(e^{i(\underline{k}-\underline{k}')\cdot\underline{R}_i} + e^{i(\underline{k}-\underline{k}')\cdot\underline{R}_j} - e^{-i\underline{k}'\cdot\underline{R}_i} e^{i\underline{k}\cdot\underline{R}_j}$$

$$- e^{i\underline{k}\cdot\underline{R}_i} e^{-i\underline{k}'\cdot\underline{R}_j}) b^*_{\underline{k}} b_{\underline{k}'} + \sum_{\underline{k}} e^{i\underline{k}\cdot(\underline{R}_j - \underline{R}_i)}], \qquad (35)$$

where we have used the commutation rules of Equations 31. Now $\sum_{(i,j)} = \frac{1}{2}\sum'_{ij}$ and $\sum_i J_{ij} = J_j \sum_{ji}$ where J_j is the same as J_{ij} but with some fixed origin in place of $\underline{R}_i$. So the last term of Equation 35 is just a constant which we will drop for now, and

$$H = \frac{S}{2N}\sum_j J_j \sum_{\underline{k}\underline{k}'}(N\delta_{\underline{k},\underline{k}'} + N\delta_{\underline{k},\underline{k}'}$$

$$- 2\sum_i e^{-i\underline{k}'\cdot\underline{R}_i} e^{i\underline{k}\cdot\underline{R}_j}) b^*_{\underline{k}} b_{\underline{k}'}. \qquad (36)$$

$$\sum_i e^{-i\underline{k}'\cdot\underline{R}_i} e^{i\underline{k}\cdot\underline{R}_j} = \sum_i e^{i(\underline{k}-\underline{k}')\cdot\underline{R}_i} e^{i\underline{k}\cdot\underline{R}_{ji}}$$

$$= N\delta_{\underline{k},\underline{k}'} e^{i\underline{k}\cdot\underline{R}_j} \tag{37}$$

So

$$H = S \sum_j J_j \sum_{\underline{k}} (1 - e^{i\underline{k}\cdot\underline{R}_j}) b^*_{\underline{k}} b_{\underline{k}}. \tag{38}$$

And referring back to Equation 23 we see that

$$H = S \sum_{\underline{k}} [F(0) - F(\underline{k})] b^*_{\underline{k}} b_{\underline{k}}. \tag{39}$$

So that $\omega(\underline{q}) = S[F(0) - F(\underline{q})]$. (40)

An alternative derivation of the magnon spectrum, Equation 40, makes use of the physical meaning of the magnon operators, $b^*_{\underline{q}}$ and $b_{\underline{q}}$. It became clear in Equation 33 that the b's were magnon operators such that $b^*_{\underline{q}}|0)$ is the one-magnon state for a magnon of wave-vector $\underline{q}$. Then we can see that the magnon energy must satisfy

$$Hb^*_{\underline{q}}|0) - b^*_{\underline{q}}H|0) = \omega(\underline{q})\ b^*_{\underline{q}}|0),$$

i.e. $$[H, b^*_{\underline{q}}]|0) = \omega(\underline{q})\ b^*_{\underline{q}}|0). \tag{41}$$

We can then evaluate the commutator of Equation 41 to find $\omega(\underline{q})$. The result is, of course, identical with Equation 40.

The magnon energies are $\hbar\omega(\underline{q})$ with $\omega(\underline{q})$ given by Equation 40 for the ferromagnetic ground state. If these energies are not positive for all $\underline{q}$, there will be an instability in the ferromagnetic ground state, and some other type of ground state will actually occur. Equation 40 shows that we will

have a negative magnon energy whenever we have $F(\underline{q})$ greater than $F(0)$ for some $\underline{q}$. In the next section we relate the stable magnetic state of the system to the maximum in $F(\underline{q})$.

Determination of the Stable Magnetic Structure

Villain (1959) has treated the problem of determining the stable magnetic structure of a metal neglecting all interactions (e.g. magnetoelastic) except the exchange interaction. We will follow his statistical mechanical treatment here. The starting point is an effective field approximation in which we take the effect of the ion at a point $\underline{R}_i$ on the spin orientation at that point to be equivalent to a magnetic field proportional to the effect at the site i of all the moments in the lattice, so that

$$\underline{h}(\underline{R}_i) = \frac{2}{g\mu_B} \sum_j J_{ij}\, \underline{S}_j, \tag{42}$$

where g is the gyromagnetic ratio (= 2), μ_B is the Bohr magneton, and J_{ij} is the exchange interaction. The usual statistical mechanical treatment shows that $\underline{S}_i$ satisfies the equation

$$\underline{S}_i = \underline{u}_i S B_S\left(\frac{g\mu_B S}{k_B T} \left|\underline{H}(\underline{R}_i)\right|\right), \tag{43}$$

where B_S is the Brillouin function for spin S, k_B is the Boltzmann constant, and

$$\underline{u}_i = \frac{\underline{H}(\underline{R}_i)}{\left|\underline{H}(\underline{R}_i)\right|} \tag{44}$$

We take the case where $|\underline{S}_i| \ll S$, i.e. near the ordering temperature so that $g\mu_B S|\underline{H}(\underline{R}_i)| \ll k_B T$ and the argument of B_S in Equation 43 is small. For small y,

$$B_S(y) \approx \frac{(S+1)}{3S}\, y. \tag{45}$$

Therefore, Equation 43 is linearized as follows:

$$\underline{S}_i = \frac{2S(S+1)}{3k_B T} \sum_j J_{ij}\, \underline{S}_j. \tag{46}$$

We can Fourier transform this equation using $F(\underline{q})$ as defined in Equation 23, the Fourier transform of J_{ij}, and defining the $\underline{q}$-dependent magnetization as

$$\underline{\sigma}(\underline{q}) = \sum_i \underline{S}_i e^{i\underline{q}\cdot\underline{R}_i}, \tag{47}$$

so that

$$\underline{\sigma}(\underline{q}) = \frac{2S(S+1)}{3k_B T} F(\underline{q})\, \underline{\sigma}(\underline{q}). \tag{48}$$

The systems of equations defined in Equations 46 and 48 have nontrivial solutions only below some critical temperature, T_o, such that

$$k_B T_o = \frac{2S(S+1)}{3} F(\underline{Q}), \tag{49}$$

$F(\underline{Q})$ being the maximum of $F(\underline{q})$. For simplification here, and also because this is the case for the experimentally observed structures in the rare earths, we will take $\underline{Q}$ so that there are only two vectors, $\pm\underline{Q}$, in the Brillouin zone for which F is maximum. Then at $T = T_o$, Equation 46 becomes

$$\underline{S}_i \sum_j J_{ij}\left[e^{i\underline{Q}\cdot(\underline{R}_j-\underline{R}_i)} + e^{-i\underline{Q}\cdot(\underline{R}_j-\underline{R}_i)}\right] = \sum_j J_{ij}\underline{S}_j, \tag{50}$$

for which we have solutions of the form:

$$S_i^\alpha = \lambda_\alpha \cos (\underline{Q}\cdot\underline{R}_i - \varphi_\alpha), \tag{51}$$

with $\alpha = x,y,z$.

When we put Equation 51 into the effective field of Equation 42, we obtain

$$\underline{h}(\underline{R}_i) = \frac{2}{g\mu_B} F(\underline{Q})\underline{S}_i. \tag{52}$$

So we can treat the problem in terms of an effective field proportional to the magnetization at a particular lattice point.

Now we need to consider the stability of magnetic structures of the form of Equation 51. The free energy of the system is

$$E = k_B T \sum_i \int_o^{S_i/S} B_S^{-1}(x)dx - \sum_{ij} J_{ij}\, \underline{S}_i\cdot\underline{S}_j + C \tag{53}$$

$$\approx \frac{3k_B T}{2S(S+1)} \sum_i \underline{S}_i^2 - \sum_{ij} J_{ij}\, \underline{S}_i\cdot\underline{S}_j + C. \tag{54}$$

The equilibrium condition, $\partial E/\partial S_i^\alpha = 0$, gives Equation 46. Taking the second derivative of E, we obtain

$$\frac{\partial^2 E}{\partial S_i^\alpha \partial S_j^\beta} = \frac{3k_B T_o}{S(S+1)} \delta_{\alpha\beta}\, \delta_{ij} - 2J_{ij}\, \delta_{\alpha\beta}. \tag{55}$$

The variation, δE, in free energy for small variations $\delta\underline{S}_i$ is

$$\delta E = \frac{1}{2} \sum_{ij} \sum_{\alpha\beta} \frac{\partial^2 E}{\partial S_i^\alpha \partial S_j^\beta} \delta S_i^\alpha \delta S_j^\beta = \frac{3k_B T_o}{2S(S+1)} \sum_i (\delta \underline{S}_i)^2 - \sum_{ij} J_{ij}\, \delta \underline{S}_i \cdot \delta \underline{S}_j$$

$$= \sum_{ij} [F(\underline{Q})\delta_{ij} - J_{ij}] \delta \underline{S}_i \cdot \delta \underline{S}_j$$

$$= \sum_i [F(\underline{Q}) - F(0)](\delta \underline{S}_i)^2. \qquad (56)$$

So δE is non-negative, and the spin system of Equation 51 will be stable.

By a proper choice of axes, Equations 51 can be rewritten as

$$S_i^x = \lambda_x \cos(\underline{Q}\cdot\underline{R}_i - \varphi),$$
$$S_i^y = \lambda_y \sin(\underline{Q}\cdot\underline{R}_i), \qquad (57)$$
$$S_i^z = 0.$$

This spin system has three different basic forms: 1) helical, with $\lambda_x = \lambda_y = s$ and $\varphi = 0$; 2) ferromagnetic or antiferromagnetic commensurate with the lattice, $\lambda_x = s$, $\lambda_y = 0$, $\varphi = 0$; 3) a more complicated periodic structure of wave vector $\underline{Q}$ for which other considerations are necessary to determine the exact structure. We will see that these various magnetic structures occur in the rare earths, and the present work seeks to find the wave vector $\underline{Q}$ for the rare earth case.

We are also interested in the generalized susceptibility, $\chi(\underline{q})$, of the conduction electron system. We can write the magnetic energy of the conduction electrons in terms of $\chi(\underline{q})$

and an effective field which polarizes the electron gas as follows:

$$H = -\frac{1}{2}\sum_{\underline{q}} |\underline{h}_{\underline{q}}|^2 \chi(\underline{q}), \tag{58}$$

with

$$\underline{h}_{\underline{q}} = \frac{J}{\mu_B\sqrt{N}} \sum_i \underline{S}_i \, e^{i\underline{q}\cdot\underline{R}_i}. \tag{59}$$

In Equation 59 $\underline{h}_{\underline{q}}$ is the Fourier transform of the effective field at $\underline{R}_i$ acting on the electrons:

$$\underline{h}(\underline{R}_i) = \frac{J}{\mu_B}\underline{S}_i. \tag{60}$$

J is an exchange parameter; N is the number of atoms in the crystal. We can now put Equation 59 into Equation 58 to obtain

$$H = -\frac{J^2}{2\mu_B^2 N} \sum_{ij} \underline{S}_i\cdot\underline{S}_j \sum_{\underline{q}} e^{i\underline{q}\cdot(\underline{R}_i-\underline{R}_j)} \chi(\underline{q}). \tag{61}$$

Our previous consideration of the s-f interaction showed that it could be expressed as a spin-spin Hamiltonian of the form (Equation 20):

$$H = -\frac{1}{2}\sum_{ij} J_{ij}\,\underline{S}_i\cdot\underline{S}_j. \tag{62}$$

We equate Equations 61 and 62 to find that, apart from constant factors which we drop for future convenience, $\chi(\underline{q})$ is just the Fourier transform of J_{ij}, so

$$\chi(\underline{q}) = F(\underline{q}). \tag{63}$$

In the next section we will discuss $\chi(\underline{q})$ from the point of view of Kubo's general linear response formalism, but we see here that we can identify it with $F(\underline{q})$ derived earlier,

Equation 24, and hence the maximum in $\chi(\underline{q})$ will determine the stable magnetic structure of a metal. We should note that, in Equation 24, we have used paramagnetic energy bands to express $F(\underline{q})$, and now $\chi(\underline{q})$. In order for these bands to be the correct ones to use in $\chi(\underline{q})$, the polarizing field of Equation 59 must be weak. Equations 47 and 59 show that the polarizing field is proportional to the magnetization. Therefore, $\underline{h}_{\underline{q}}$ will be weak only very near the critical temperature, and so our calculation applies only to the initial ordering of the ionic spins.

Generalized Susceptibility

A very general treatment of linear response in solids, including the generalized magnetic susceptibility, was given by Kubo (1957). We will restrict our treatment to the points of interest in this work, i.e. the $\underline{q}$-dependent magnetic susceptibility omitting consideration of any frequency dependence (so $\omega = 0$ here). It should be pointed out here that besides Kubo's paper there are excellent discussions of linear response formalism in Kittel (1963) and Tyablikov (1967).

We begin by assuming a Hamiltonian of the form

$$H = H_o + H'(t),$$

$$H'(t) = -\underline{M}\cdot\underline{h}\, e^{i\underline{q}\cdot\underline{r}} e^{\epsilon t/\hbar}. \qquad (64)$$

We want to look at the system at zero temperature because we are not interested in the effect of temperature in this particular problem. In this case we are only interested in the

ground state: $|G) = U(0,-\infty)|0)$, where $|0)$ is the unordered ground state of H_o and $U(t,t_o)$ is the time development operator from time t_o to time t. (See, for example, Messiah (1961) where he calls this the "evolution operator.") Also, we are interested in linear response, so we will look only at linear terms in the expansion for the susceptibility. We want to know the response to a field whose spatial variation is described by a wave vector $\underline{q}$, so we will Fourier analyze the magnetization to look at the $\underline{q}^{th}$ Fourier component of the susceptibility. Then $\underline{M}_{\underline{q}} = \chi(\underline{q})\underline{h}_{\underline{q}}$, and the system is isotropic to the spins, so we can consider only z-components of $\underline{M}$ and $\underline{h}$, obtaining $\chi(\underline{q}) = M^z_{\underline{q}}/h^z_{\underline{q}}$. H_o describes a nonmagnetized system, and we want to know what is the magnetization, $\underline{M}$, that takes place with a small field applied as a perturbation; therefore, we can look at the response in the interaction picture:

$$U_I(0,-\infty) = 1 - \frac{i}{\hbar}\int_{-\infty}^{0} H'_I(t)dt + \text{higher terms}, \tag{65}$$

$$H'_I(t) = e^{iH_o t/\hbar} H'(t) e^{-iH_o t/\hbar}. \tag{66}$$

Then the expectation value of the magnetization is

$$M_z = (G|M_z|G) = (0|(1 + \frac{i}{\hbar}\int_{-\infty}^{0} H'_I(t)dt)\, M_z \,(1 - \frac{i}{\hbar}\int_{-\infty}^{0} H'_I(t)dt)|0)$$

$$= (0|M_z|0) + \frac{i}{\hbar}\int_{-\infty}^{0} (0|[H'_I(t),M_z]|0)dt. \tag{67}$$

The first term in this equation is zero since $|0)$ is unmagnetized. We will consider the two parts of the commutator in the second term separately so $[\ ,\ ] = (I) - (II)$. First, we write M_z in second quantization language:

$$M_z(\underline{r}) = \frac{1}{2N} \sum_{\underline{k}\underline{k}'} \sum_{nn'} e^{i(\underline{k}-\underline{k}')\cdot\underline{r}} u^*_{\underline{k}',}(\underline{r}) u_{\underline{k}}(\underline{r})(c^*_{\underline{k}'n'+} c_{\underline{k}n+} - c_{\underline{k}'n'-} c_{\underline{k}n-}), \tag{68}$$

where the $u_{\underline{k}}(\underline{r})$ are Bloch functions with the lattice periodicity. Then

$$(I) = - e^{iH_o t/\hbar} \frac{1}{2\pi} \int d\underline{r}' M_z(\underline{r}') h_z e^{i\underline{q}\cdot\underline{r}'} e^{\epsilon t/\hbar} e^{-iH_o t/\hbar} M_z(\underline{r}). \tag{69}$$

But $e^{iH_o t/\hbar} M_z e^{-iH_o t/\hbar}$ is just the interaction representation form for M_z, and in that case we get operators $c^*(t)$ and $c(t)$ in Equation 68, where $c^*_{\underline{k}nm}(t) = e^{iE_n(\underline{k})t/\hbar} c^*_{\underline{k}nm}$ and $c_{\underline{k}nm}(t) = e^{-iE_n(t)/\hbar} c_{\underline{k}nm}$. So we can pull out the time dependence to do the time integral of Equation 67 separately. Now

$$(0|(I)|0) = - \frac{1}{2\pi} \int d\underline{r}' \frac{h_z e^{i\underline{q}\cdot\underline{r}'}}{4N^2} \sum_{\underline{k}\underline{k}'} \sum_{nn'} \sum_{\underline{k}_1\underline{k}_2} \sum_{n_1 n_2}$$

$$e^{i[E_{n'}(\underline{k}')-E_n(\underline{k})]t/\hbar} e^{\epsilon t/\hbar} e^{i(\underline{k}-\underline{k}')\cdot\underline{r}'} u^*_{\underline{k}'n'}(\underline{r}')\, u_{\underline{k}n}(\underline{r}')$$

$$e^{i(\underline{k}_1-\underline{k}_2)\cdot\underline{r}} u^*_{\underline{k}_2 n_2}(\underline{r})\, u_{\underline{k}_1 n_1}(\underline{r})(0|(c^*_{\underline{k}'n'+} c_{\underline{k}n+} - c^*_{\underline{k}'n'-} c_{\underline{k}n-})$$

$$(c^*_{\underline{k}_2 n_2+} c_{\underline{k}_1 n_1+} - c^*_{\underline{k}_2 n_2-} c_{\underline{k}_2 n_2-})|0). \tag{70}$$

We use Equation 11 to evaluate the matrix element above and do the sums on n_1, n_2, $\underline{k}_1$, and $\underline{k}_2$. We can also do the integral

on $\underline{r}'$ as follows:

$$\int d\underline{r}'\, e^{i\underline{q}\cdot\underline{r}'}\, e^{i(\underline{k}-\underline{k}')\cdot\underline{r}'}\, u^*_{\underline{k}',n'}(\underline{r}')\, u_{\underline{k}n}(\underline{r}')$$

$$= \sum_i e^{i(\underline{k}-\underline{k}'+\underline{q})\cdot\underline{R}_i} \int_{\text{cell}} d\underline{r}\, e^{i(\underline{k}-\underline{k}'+\underline{q})\cdot\underline{r}}\, u^*_{\underline{k}',n'}(\underline{r})\, u_{\underline{k}n}(\underline{r})$$

$$= N\,\delta(\underline{k}'-\underline{k}-\underline{q}-\underline{K}_o)\, K_{nn'}(\underline{k},\underline{k}+\underline{q}+\underline{K}_o), \tag{71}$$

where

$$K_{nn'}(\underline{k},\underline{k}+\underline{q}+\underline{K}_o) = \int_{\text{cell}} d\underline{r}\, e^{-i\underline{K}_o\cdot\underline{r}}\, u^*_{\underline{k}+\underline{q}+\underline{K}_o n'}(\underline{r})\, u_{\underline{k}n}(\underline{r}). \tag{72}$$

We then put this into Equation 67 and Fourier transform on $\underline{r}$ to get a second term like Equation 71 and finally obtain

$$M_z^{(I)}(\underline{q}) = -\frac{i}{4N\hbar} \sum_{\underline{k}} \sum_{nn'} K^2_{nn'}(\underline{k},\underline{k}+\underline{q}+\underline{K}_o) h_z\, 2f_{\underline{k}n}(1-f_{\underline{k}+\underline{q}+\underline{K}_o n'})$$

$$\int_{-\infty}^{o} e^{-i[E_{n'}(\underline{k}+\underline{q}+\underline{K}_o)-E_n(\underline{k})]t/\hbar}\, e^{\epsilon t/\hbar}\, dt \tag{73}$$

$$= -\frac{i}{2N\hbar} h_z \sum_{\underline{k}} \sum_{nn'} K^2_{nn'}(\underline{k},\underline{k}+\underline{q}+\underline{K}_o) \frac{f_{\underline{k}n}(1-f_{\underline{k}+\underline{q}+\underline{K}_o n'})}{-\frac{i}{\hbar}[E_{n'}(\underline{k}+\underline{q}+\underline{K}_o)-E_n(\underline{k})]+\frac{\epsilon}{\hbar}}$$

$$= \frac{h_z}{2N} \sum_{\underline{k}} \sum_{nn'} K^2_{nn'} \frac{f_{\underline{k}n}(1-f_{\underline{k}+\underline{q}+\underline{K}_o n'})}{E_{n'}(\underline{k}+\underline{q}+\underline{K}_o)-E_n(\underline{k})+i\epsilon}. \tag{74}$$

In a similar way we find

$$M_z^{(II)}(\underline{q}) = -\frac{h_z}{2N} \sum_{\underline{k}} \sum_{nn'} K^2_{nn'} \frac{f_{\underline{k}n}(1-f_{\underline{k}+\underline{q}+\underline{K}_o n'})}{E_{n'}(\underline{k}+\underline{q}+\underline{K}_o)-E_n(\underline{k})-i\epsilon}. \tag{75}$$

Then

$$\chi(\underline{q}) = \frac{1}{2N} \sum_{\underline{k}} \sum_{nn'} K^2_{nn'}(\underline{k},\underline{k}+\underline{q}+\underline{K}_o)\, f_{\underline{k}n}(1-f_{\underline{k}+\underline{q}+\underline{K}_o n'})$$

$$\left[\frac{1}{E_{n'}(\underline{k}+\underline{q}+\underline{K}_o) - E_n(\underline{k})+i\epsilon} + \frac{1}{E_{n'}(\underline{k}+\underline{q}+\underline{K}_o) - E_n(\underline{k}) - i\epsilon}\right]$$

$$= \frac{1}{N} \sum_{\underline{k}} \sum_{nn'} K^2_{nn'}(\underline{k},\underline{k}+\underline{q}+\underline{K}_o)\, f_{\underline{k}n}(1-f_{\underline{k}+\underline{q}+\underline{K}_o n'})$$

$$\frac{[E_{n'}(\underline{k}+\underline{q}+\underline{K}_o)-E_n(\underline{k})]}{[E_{n'}(\underline{k}+\underline{q}+\underline{K}_o)-E_n(\underline{k})]^2 + \epsilon^2}. \qquad (76)$$

We have assumed ϵ small in which case Equation 76 is just the definition of the principle-value integral, so we finally have

$$\chi(\underline{q}) = \frac{1}{N} \Sigma' \sum_{\underline{k}} \sum_{nn'} K^2_{nn'}(\underline{k},\underline{k}+\underline{q}+\underline{K}_o)\, \frac{f_{\underline{k}n}(1-f_{\underline{k}+\underline{q}+\underline{K}_o n'})}{E_{n'}(\underline{k}+\underline{q}+\underline{K}_o) - E_n(\underline{k})}, \qquad (77)$$

where we use Σ' to mean that we take principle values whenever the denominator goes to zero.

We see that except for the matrix elements, K^2 or I^2, $\chi(\underline{q})$ is the same as $F(\underline{q})$ in Equation 24. We showed in the last section of this chapter that $\chi(\underline{q})$ should be the same as $F(\underline{q})$ and that the energy of the spin system goes as the negative of these quantities. We now see how $\chi(\underline{q})$ is just the linear response of the system to a small $\underline{q}$-dependent field. We will make the approximation that the matrix elements, K and I, are constant and will factor them out. For the rest of this work we will refer to

$$\frac{1}{N} \Sigma' \sum_{\underline{k}} \sum_{nn'} \frac{f_{\underline{k}n}(1-f_{\underline{k}+\underline{q}+\underline{K}_o n'})}{E_{n'}(\underline{k}+\underline{q}+\underline{K}_o) - E_n(\underline{k})} \qquad (78)$$

as $\chi(q)$. χ will then have the dimensions of the density of states (states/Rydberg/atom) for the purposes of this investigation.

Application to the Rare Earths

As we mentioned previously, the f-shells of the rare-earth atoms in the metals have radii of the order of one-tenth of the nearest-neighbor distances so that there is no significant overlap between atoms in the crystal. Because of this fact we know that the mechanism for magnetic ordering must involve the conduction electrons, and therefore the s-f indirect-exchange interaction should be applicable to the rare earths. So, in principle, we want to calculate the eigenvalues and eigenfunctions of the indirect-exchange Hamiltonian in the case where the spins occupy the site of a regular crystal structure, such as hexagonal-close-packed (hcp) for the heavy rare earths we have considered in this work. (In the rest of this discussion the term "rare earths" will be used to refer to the particular heavy rare earths we have studied in the present calculation, i.e. gadolinium, dysprosium, erbium, and lutetium.)

In the rare earths we find that the angular momentum of the 4f-shell is not significantly quenched, as can be observed by measuring the magnetic moment of an essentially free rare-earth ion in a nonmagnetic matrix and comparing it with the measured moment per ion of the metal. The angular momentum that is specified in this case is $\underline{J}$ and not simply $\underline{S}$. The

magnetic degrees of freedom of each atom are described by 2j+1 eigenfunctions rather than 2s+1. To take this effect into account, we make use of the Lande g-factor. For states of definite j we have

$$(jm|\underline{M}_i|jm') = g_i\ (jm|\underline{J}_i|jm') = (jm|\underline{J}_i + \underline{S}_i|jm'),$$

where $\underline{M}_i$ is the magnetic moment operator of the ion. The exchange interaction couples only the spins of the ions with the spins of the conduction electrons, so in the interaction Hamiltonian we simply replace $\underline{S}_i$ by $(g_i-1)\underline{J}_i$ (unless $j = 0$). The factor (g_i-1) may be either positive or negative and acts as a sort of "spin charge," allowing an extra degree of freedom in alloyed magnetic rare earths. De Gennes (1958) was the first to point out that S should be replaced by $(g-1)J$ and Liu (1961a) discussed this point in more detail. For future reference, we have given relevant angular momentum data for the rare earths in Table 1.

We show the magnetic structures for those of the heavy rare earths which have some periodic antiferromagnetic phase in Figure 2 (Koehler 1965). Gadolinium has only a ferromagnetic phase, and lutetium has no moment, so these are not included in the figure. As can be seen from the figure, all these periodic magnetic structures can be described by a wave vector $\underline{q}$ which has only a z-component. This is also true for lutetium when a small amount of some other element such as terbium is added to provide a moment (Child et al. 1965).

Table 1. Angular momenta and g-factors of rare earths

Number of electrons in f-shell	Rare earth	s	l	j	g-1	(g-1)j
7	Gd	7/2	0	7/2	1	7/2
8	Tb	3	3	6	1/2	3
9	Dy	5/2	5	15/2	1/3	5/2
10	Ho	2	6	8	1/4	2
11	Er	3/2	6	15/2	1/5	3/2
12	Tm	1	5	6	1/6	1
14	Lu	0	0	0	...	...

Therefore, the interesting part of $\chi(\underline{q})$ will be for $\underline{q} = (0,0,q)$, for it is in this region that the maximum in χ should occur to stabilize the energy of one of the magnetic structures of Figure 2. The Brillouin zone for the hexagonal lattice is shown with the symmetry points and lines labeled in the usual way in Figure 3. In the notation of that figure, then, the interesting range of $\underline{q}$'s is from Γ to A. In all later discussions we will confine ourselves only to $\chi(q)$ where it is understood that q is the magnitude of a wave-vector $\underline{q}$ which is chosen along the line Γ to A.

The hcp crystal structure has two atoms in the unit cell. Therefore, the susceptibility, $\chi(q)$, will have two branches in the primitive Brillouin zone. These two branches correspond to two different combinations of the two allowed kinds of

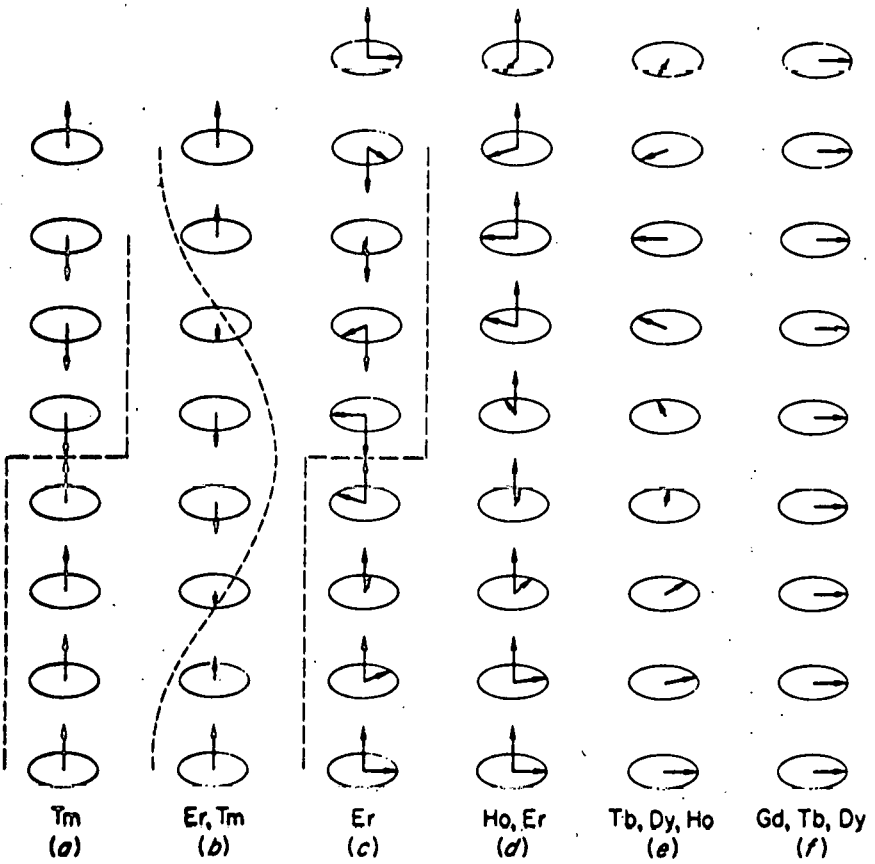

Figure 2. Magnetic structures of rare-earth metals

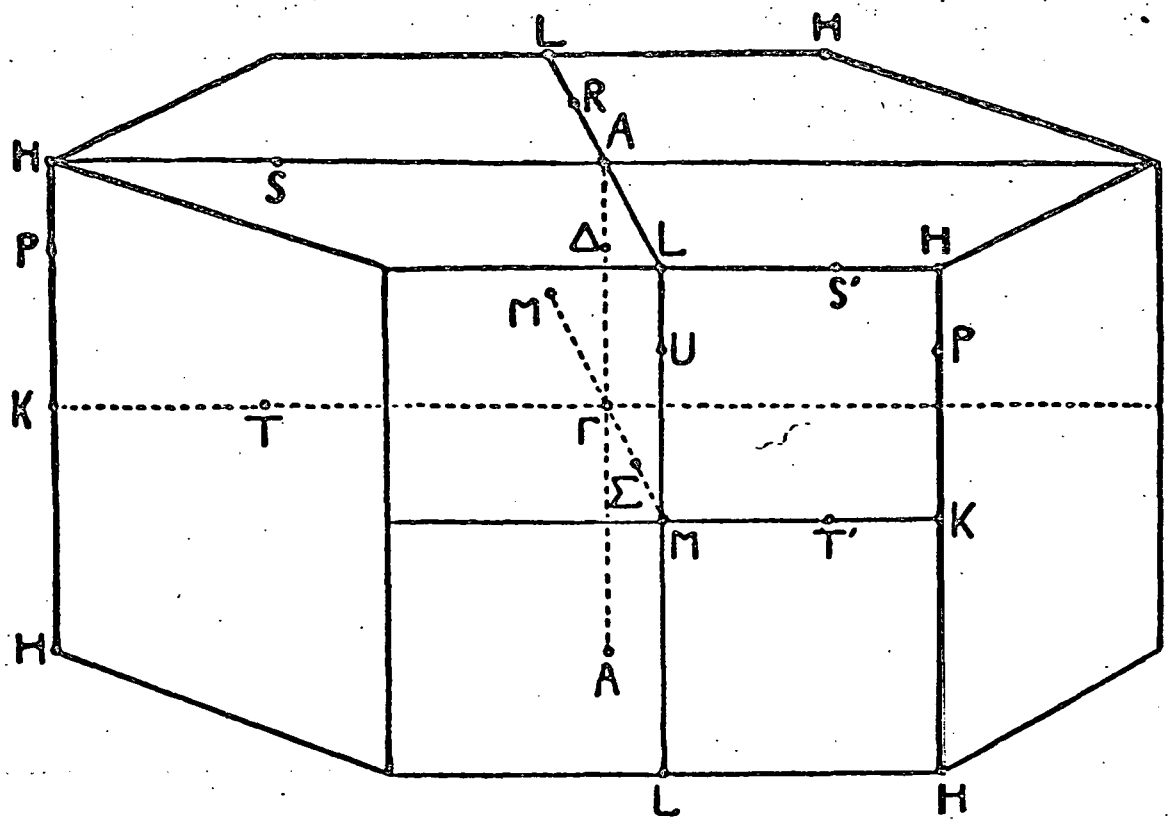

Figure 3. Brillouin zone for the hexagonal-clcse-packed crystal structure

coupled initial and final states, $\underline{k}$ and $\underline{k}+\underline{q}$ in the expression derived earlier for $\chi(q)$, Equation 78. Watson et al. (1968) point out that, if spin-orbit coupling is ignored, the allowed coupling corresponds to coupling 1) within the same band inside the first zone and 2) between adjacent bands from the first to the second zone. These are just the kinds of coupling obtained naturally in the double-zone representation for the bands; therefore, we need to fold out the electron bands to perform the evaluation of $\chi(q)$ in the double-zone scheme. The question then arises as to the validity of this folding out of the bands. If there is no spin-orbit coupling, the structure factor is everywhere zero on the AHL zone face, and the folding out of the bands into the double zone is a correct procedure (Mott and Jones 1958). In fact when spin-orbit coupling is neglected, the double-zone representation is the one most often used because of its convenience. However, the introduction of spin-orbit coupling produces gaps in the electron bands on the AHL face of the Brillouin zone and raises questions about the validity of the double-zone scheme. The largest gaps are at the point H of the zone, while they go to zero along the line A to L (Cohen and Falicov 1960). Examination of the gap at H shows that it is quite small relative to typical band widths. In fact, the numerical convergence of the present relativistic APW bands is not quite sufficient to properly resolve the splitting (Keeton 1966). This seems to

indicate that the double-zone representation is probably quite a good approximation even with the relativistic energy bands we are using. We should note, however, that the relativistic band calculation does introduce changes in the relative shapes and spacings of the bands which are important to this investigation, particularly as they are reflected in the rather significant differences in the Fermi surfaces from what is calculated nonrelativistically (Keeton 1966).

To conclude our discussion of the considerations needed to properly apply the ideas of generalized susceptibility and indirect exchange to the rare earths, we present the ordering temperatures and the experimentally determined magnetic wave vectors, Q, for the heavy rare earths at their initial ordering points in Table 2 which is made up from information reported by Koehler (1965). In the rest of this work we will refer to the stable magnetic q, the maximum in $\chi(q)$, as Q.

Table 2. Magnetic ordering properties of the heavy rare-earth metals: the Neel temperature (T_N), the Curie temperature (T_C), the paramagnetic Curie temperature (θp), the interlayer turn angle at the initial ordering point (ω_i), and the magnetic wave vector at the initial ordering point (Q). (The periodic structure for lutetium is extrapolated from data for Tb-Lu alloys. The information in this table is taken from Koehler 1965.)

Metal	$T_N(^oK)$	$T_C(^oK)$	$\theta_P(^oK)$	ω_i(deg.)	Q(π/c)
Gd	...	293.2	317	0	0
Tb	229	221	224	20.5	.23
Dy	178.5	85	153	44	.49
Ho	132	20	83	51	.57
Er	85	19.6	42	51.4	.57
Tm	55	22	20	51.4	.57
Lu	...	...	...	48	.53

NUMERICAL CALCULATION OF THE GENERALIZED SUSCEPTIBILITY

General Considerations

We recall the form of the generalized susceptibility from Equation 78:

$$\chi(q) = \frac{1}{N} \sum_{\underline{k}nn'}' \frac{f_{\underline{k}n}(1-f_{\underline{k}+\underline{q}+\underline{K}_o n'})}{E_{n'}(\underline{k}+\underline{q}+\underline{K}_o) - E_n(\underline{k})}. \qquad (78)$$

The f_{kn} are Fermi-Dirac functions and are quite close to step functions of value 1 for $E_n(\underline{k})$ smaller than E_F and of value 0 for $E_n(\underline{k})$ greater than E_F throughout the temperature range we are concerned with. In fact, the smearing of the $f_{\underline{k}n}$ with increasing temperature only has an effect on the susceptibility of the order of $(kT/E_F)^2$, which is very small in all the cases we are considering. Keeton and Loucks (1968) find E_F to be typically about 0.4 Rydberg above the bottom of the bands, which gives $E_F/k \sim 10^5$ °K, a much higher temperature than any in Table 2. We will assume in the future that the $f_{\underline{k}n}$ are simply the step functions described here.

The energy bands in Equation 78 must be provided numerically. We have used bands calculated by Keeton and Loucks (1968) using the relativistic-augmented-plane-wave method for gadolinium, dysprosium, erbium, and lutecium. The bands for dysprosium and erbium were each calculated twice, using two different potentials. Keeton and Loucks have labeled these Dy1, Dy2, Er1, and Er2; we will use the same labels and

consider all six sets of bands. The bands for Dy2 are typical of the whole series and are given in Figure 4.

When we consider a macroscopic crystal with of the order of 10^{23} atoms, there are 10^{23} points $\underline{k}$ in the Brillouin zone over which we must perform the summation of Equation 78. For all practical purposes, this is a continuous distribution of states $\underline{k}$ in the zone and the sum can be changed to a principal-value integral. The summations over the bands are relatively easy to perform since we only deal, in general, with a small number of bands. For example, the rare-earths are tri-valent, so there are one and one-half bands below the Fermi energy (in the double-zone scheme) and, in the case of Dy2 shown in Figure 4, two and one-half bands above the Fermi energy have been calculated, for a total of four bands. Higher bands are likely to be very free-electron like since the potential is felt less as excitation energies become higher.

The real problem, then, in the evaluation of the susceptibility is the computation of the integral over states $\underline{k}$ for the numerical energy bands. The energy bands were actually calculated on levels 1, 3, 5, and 7 of the mesh shown in the 1/24th zone in Figure 5. With fifteen points per level we have sixty points where the bands have actually been calculated in the 1/24th zone or 1200 points in the entire zone. We are interested in obtaining as fine a mesh as possible in the k_z-direction so that we can know $\chi(q)$ at as many points on the

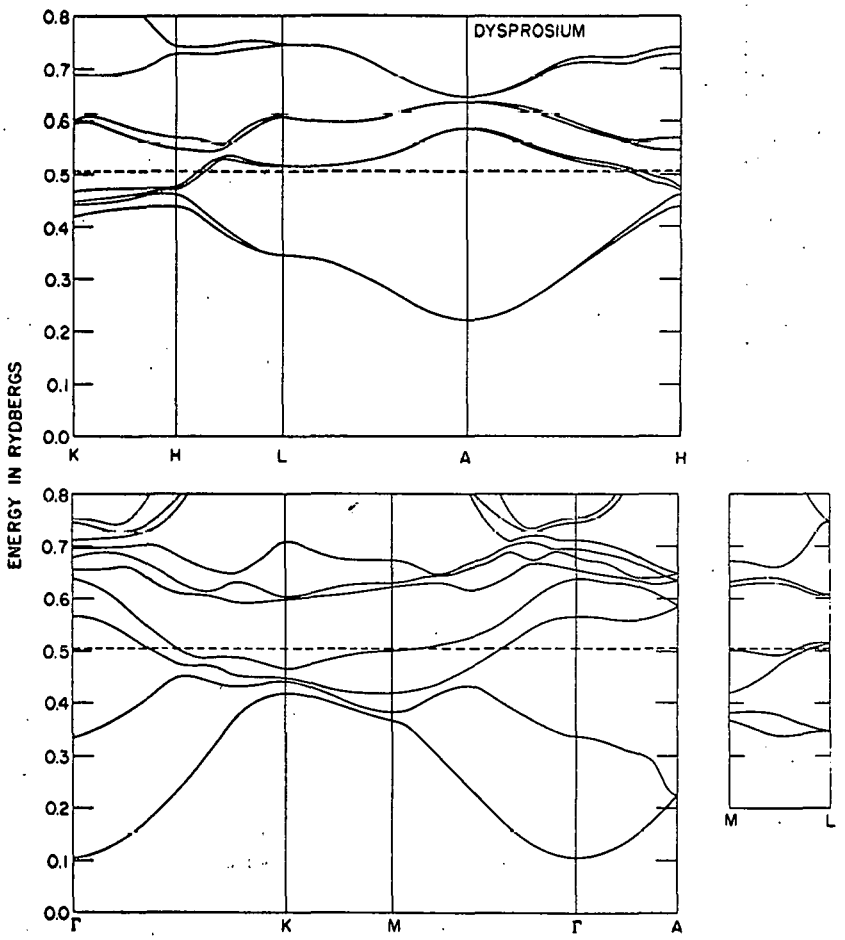

Figure 4. Energy bands for Dy2 along the symmetry axes of the Brillouin zone. The dashed line indicates the Fermi energy

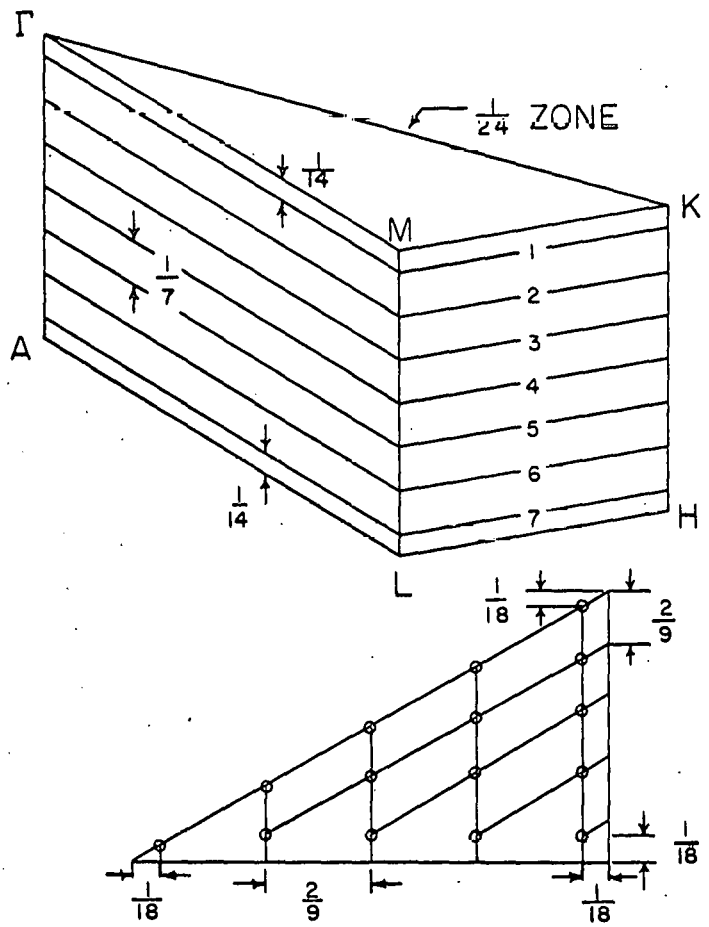

Figure 5. 1/24th Brillouin zone showing the calculation mesh

line Δ as possible. We cannot know $\chi(q)$ any better than we know $E(k_z)$ because both the points $\underline{k}$ and $\underline{k}+\underline{q}+\underline{K}_o$ must be in any mesh we use to approximate the integral of Equation 78. Given the uncertainty in the energy bands to begin with, the simplest approximation to the integral is probably as well as we need to do. This would correspond to the trapezoidal rule for ordinary one-dimensional quadrature (Pennington 1965, p. 191, for example) which in three dimensions would amount to taking each point in the mesh to be representative of the volume element at which it is centered and summing the terms of Equation 78 for each point times the differential volume of the point's volume element with respect to the whole zone. This, in fact, is what we have done after developing appropriate interpolation schemes to extend our mesh to one convenient for the calculation of $\chi(q)$ on the line Δ. The fact that we have a principal-value integral means we need to avoid zero energy denominators (as we clearly must do to compute the sum in any case). Because of this we restrict $E_n(\underline{k}) \leq E_F$ and $E_{n'}(\underline{k}+\underline{q}+\underline{K}_o) > E_F$, never allowing them to be equal. We will discuss below how well we can expect this kind of scheme to work.

The next question is how to interpolate to obtain the mesh we want. We could simply use linear or quadratic interpolations to find points between those calculated. In view of the inherent uncertainties in the bands, and hence in the whole calculation, these may not be too bad. We have, in fact,

made use of linear interpolations done by Keeton (1966) in each of the levels of Figure 5 to extend the mesh to 45 and 90 points per level. Along the k_z-direction, however, we felt that we needed to do as well as possible because it is the way in which q connects states along this direction that determines χ. The only reasonable criteria for this interpolation which would be suggested by the physical properties of the bands are that they be smooth and that they have zero slope at the zone boundaries. The standard method for doing smooth interpolations is the "spline interpolation" (Pennington 1965, p. 404) which is a good approximation to stretching a perfectly elastic, thin line through all the points, fixing the boundary conditions, and minimizing the strains. This amounts to a piecewise cubic polynomial approximation of the bands. We tried two different variations of the spline fit: one in which we used our judgment to choose the points at the zone boundaries and then required the bands to have zero slope at those points, and the other in which we did not put in the points at the zone boundaries but used the symmetry of the bands about the zone boundaries to fit them at the end points, still requiring them to have zero slope there. The results obtained for $\chi(q)$ for Dy2 in the two interpolation schemes were entirely similar in the important features, so we did all further work using the second scheme which is the easier to apply. Using this interpolation scheme, we extended the mesh

for the energy bands from four levels in Figure 5 to twenty-nine. We believe that the criteria used in this extension of the mesh are reasonable and the interpolated bands provide as good a basis for the calculation of the susceptibility as is at present available.

Given the interpolated bands on a mesh that provides a reasonable coverage for q, and given the three-dimensional analogue of the trapezoidal rule for the integration, we can proceed to calculate the susceptibility and to consider the reliability of the results. We have done this for Dy2, and as we will see from the similarity of the final results for the other metals with those for Dy2, the conclusions we draw from various considerations in the calculation should apply to the whole set of metals we are studying.

First we considered the effect of the summations over the bands. We did the calculation in three different cases: with the four calculated bands, with the four calculated bands plus two additional free-electron bands on top, and with only the band which determines the Fermi surface. The results obtained in the three calculations contained exactly the same features in $\chi(q)$ so that the magnetic ordering Q predicted was exactly the same in all three cases. In fact, within the confidence we have in the calculation, the differences were q-independent, so that χ was shifted in magnitude only. The reason for this is that, as seen in Figure 4, the bands are rather flat, and

as we get far from the Fermi energy, the energy denominators in Equation 78 become quite small, so that each term contributes very little to $\chi(q)$ and is not able to distinguish various q's very well. In fact these small terms have a kind of random fluctuation through the whole range of q's which is q-independent on the average. In view of this result, all further calculations were done using only the bands at the Fermi surface and the summations over bands were dropped from Equation 78. Using only the bands at the Fermi surface also has the advantage of allowing a more direct comparison than would otherwise be possible of the value of $\chi(0)$ with the density of states at the Fermi energy, $N(E_F)$, as we will see below. This comparison will indicate the degree of consistency between the calculations of $\chi(q)$ and $N(E_F)$ using the same energy bands. We can examine the relationship between the density of states at the Fermi energy and $\chi(0)$ by considering the limit of $\chi(q)$ as q goes to zero:

$$\chi(0) = \lim_{q\to 0} \chi(q) = \lim_{q\to 0} \frac{1}{N} \sum_{\underline{k}}' \frac{f_{\underline{k}}(1-f_{\underline{k}+\underline{q}+\underline{K}_o})}{E(\underline{k}+\underline{q}+\underline{K}_o) - E(\underline{k})}$$

$$= \frac{1}{2N} \lim_{q\to 0} \sum_{\underline{k}}' \frac{f_{\underline{k}} - f_{\underline{k}+\underline{q}+\underline{K}_o}}{E(\underline{k}+\underline{q}+\underline{K}_o) - E(\underline{k})}. \qquad (79)$$

For small enough $\underline{q}$, we can take $\underline{K}_o = \underline{0}$, and we can use the first two terms of the Taylor expansion for $f_{\underline{k}+\underline{q}}$:

$$f_{\underline{k}+\underline{q}} = f_{\underline{k}} + [E(\underline{k}+\underline{q}) - E(\underline{k})] \frac{\partial f_{\underline{k}}}{\partial E(\underline{k})} + \ldots. \qquad (80)$$

Then

$$\chi(0) = \frac{1}{2N} \sum_{\underline{k}} \left[- \frac{\partial f_{\underline{k}}}{\partial E(\underline{k})} \right] \tag{81}$$

$$= \frac{1}{2N} \sum_{\underline{k}} \delta(E(\underline{k}) - E_F). \tag{82}$$

Equation 82 just counts all the states on the Fermi surface and divides by 2N, so

$$\chi(0) = \frac{1}{2} N(E_F). \tag{83}$$

Keeton and Loucks (1968) calculated $N(E_F)$ for their bands, and the values they obtained are given in Table 3. The uncertainties in $N(E_F)$ are rather large (of the order of 25%) because of the histogram approach to the calculation and the uncertainties in the bands to begin with, so values of $\chi(0)$ between about 10 and 18 states/Rydberg/atom would be consistent with the densities of states given in Table 3. We shall see that the limit $\lim_{q \to 0} \chi(q)$ in our calculations is consistent with $N(E_F)$.

We have shown how $\chi(0)$ is related to the density of states at the Fermi energy, $N(E_F)$. Actually, in the numerical calculation of the susceptibility $\chi(0)$ can never be calculated correctly because all the terms with denominators $E(\underline{k}) - E(\underline{k})$ are eliminated from the integral, making $\chi(0)$ go to zero. In the limit of q going to zero, however, the numerator of the integrand is also zero and the integrand has a finite limit equal to $\frac{1}{2} N(E_F)$, as we have seen above. It should be pointed out that even for small but non-zero q there may be terms that are eliminated from the integral but show up in the density of

Table 3. Density of states at the Fermi energy, $N(E_F)$, for the heavy rare earths (Keeton and Loucks 1968)

Metal	$N(E_F)$ (States/Rydberg/atom)
Gd	28.5
Dy1	27.7
Dy2	24.3
Er1	24.3
Er2	23.6
Lu	25.5

states. These terms arise from portions of the Fermi surface that are parallel to $\underline{q}$ so that there are states $\underline{k}$ and $\underline{k}+\underline{q}$ both on the Fermi surface. As we have shown for $\chi(0)$, the susceptibility due to this kind of term is just $\frac{1}{2}N(E_F)$ times the differential area of Fermi surface involved in this coupling. For a strange Fermi surface like a cube, which we will discuss further on, there will be quite a large portion of Fermi surface involved in this kind of coupling for a rather large range of q's; however, for the usual rather complicated Fermi surface, such as in the rare earths, these terms should not be very important. We will see that $N(E_F)$ gives a $\chi(0)$ which is quite consistent with the rest of the susceptibility

in the cases we have calculated, indicating that these density of states terms are insignificant except for q = 0.

The next consideration we gave to the calculation was of the effect of changing meshes in the approximation of the integral. We had ninety points interpolated in each triangular section of the 1/24th zone (Figure 5) which we divided into two groups of forty-five points each. This gave a total of 1305 points in the 1/24th zone or 2565 points in the 1/12th zone. We actually have to sum over 5130 points in 1/12th of the double zone, from Γ to A to Γ to A to Γ. This mesh is equivalent to 27,216 points in the primitive Brillouin zone. The differences in $\chi(q)$ between these two meshes were insignificant, so that we feel that the mesh chosen is fairly representative of the actual energy band system. One of the meshes fits the symmetry of the zone better than the other one, so for our final results we weighted the better mesh twice as heavily as the other one and averaged the two calculations. We will see when we discuss the susceptibility for free-electron energy bands that the choice of mesh can be important in introducing spurious peaks in the susceptibility because of the particular relationship of the chosen mesh to the Fermi surface. Our approximation to the integral over the Brillouin zone assumes that the energy at the mesh point is representative of

the energy in the volume element surrounding that point, so the Fermi functions in the integral cause it to act as if the Fermi surface does not cut any of the volume elements but goes only along the boundaries between the volume elements. In special cases this may cause severe distortions of the Fermi surface and introduce spurious features into the susceptibility. We have investigated various schemes for improving this situation and have determined that the accuracy of the bands and the inherent accuracy of the calculation of the susceptibility do not at present warrant the very considerable amount of work required to do just a little better in this regard. A simple comparison of calculations with two different meshes, however, should reveal shifts in certain features of the susceptibility if the relation of the mesh to the Fermi surface is responsible for those features. This is indeed evident in our calculations, most strikingly in the free-electron case where the effect is most severe because of the spherical shape of the Fermi surface, as we will point out in the discussion below. So comparison of the calculations with several meshes should allow us to eliminate spurious features from $\chi(q)$. In the next section we will discuss the relation between the features of the susceptibility and the geometry of the Fermi surface which will also allow us to eliminate spurious features

in $\chi(q)$ when there is no corresponding peculiarity in the Fermi surface.

Relation Between Fermi Surface Geometry and the Susceptibility

Roth et al. (1966) have used a very sophisticated treatment to show the nature of the relationship between the Fermi surface and the shape of the generalized susceptibility. We shall simply look at some different Fermi surface geometries for special bands to convey the important ideas of the theory. We shall consider three types of Fermi surface near a stationary value of q (q still being restricted to the k_z-direction which is sufficient for the purposes of this discussion): 1) spherical, where Q will be a diameter of the sphere giving coupling, or "nesting," of one point on the surface into another on the other side, 2) cylindrical, where Q will again be a diameter, but now it nests a whole line of points, and 3) parallel sheets, k_z = constant planes, so that Q nests areas into each other. We are only assuming the Fermi surfaces to be like this over a small region so a complicated real Fermi surface may contain all three types of nesting.

For the spherical Fermi surface we consider

$$\chi(q) = \frac{\Omega}{4\pi^3 N} \int d\underline{k} \, \frac{f_{\underline{k}}}{E(\underline{k}+\underline{q}) - E(\underline{k})}, \tag{84}$$

and we will omit all constant factors from here on. We will choose the origin of coordinates in $\underline{k}$-space such that Q is

along the k_z-axis, and sufficiently close to the Fermi surface we will take $E(\underline{k}) = k^2$. So

$$\chi(q) \propto \int(\text{over points far from the Fermi surface}) + \int_{k_F-\Delta k}^{k_F} k^2 dk \int_{-1}^{-1+\Delta\mu} d\mu \frac{1}{(\underline{k}+\underline{q})^2 - k^2}. \quad (85)$$

We want to see the effect of nesting points, so dropping the first term we have

$$\chi(q) \propto \frac{1}{q} \int_{k_F-\Delta k}^{k_F} k^2 dk \int_{-1}^{-1+\Delta\mu} \frac{d\mu}{2k\mu + q}$$

$$\propto \frac{1}{q} \int_{k_F-\Delta k}^{k_F} k dk \ln \left| \frac{q + 2k(\Delta\mu-1)}{q - 2k} \right|.$$

But $q = Q + \delta q = 2k_F + \delta q$, so

$$\chi(\delta q) \propto \text{constants} + \delta q \ln \left| \frac{\delta q}{2\Delta k + \delta q} \right|. \quad (86)$$

When δq goes to zero, χ goes to a constant, but its slope goes to $-\infty$. We see, however, that this type of nesting does not produce a maximum in the susceptibility at Q. In fact, the slope is everywhere negative for the part of χ due to a spherical piece of Fermi surface which indicates that the ferromagnetic state would tend to stabilize when only point to point nesting exists on the Fermi surface.

For the cylindrical Fermi surface we again use Equation 84, but we will do the integral in cylindrical coordinates with the cylindrical axis the k_x-axis. Choose the origin of coordinates such that Q is along the k_z-axis and take $E(\underline{k}) = k^2$

sufficiently close to the Fermi surface. Then

$$\chi(q) \propto \int \text{(over points far from the Fermi surface)} + \int_{-L}^{L} dk_x \int_{k_F-\Delta k}^{k_F} kdk \int_{\pi-\Delta\theta}^{\pi+\Delta\theta} d\theta \frac{1}{2kq\cos\theta + q^2}. \quad (87)$$

Dropping the first term,

$$\chi(q) \propto \frac{1}{q} \int_{k_F-\Delta k}^{k_F} kdk \int_{o}^{\Delta\theta} \frac{d\alpha}{q - 2k\cos\alpha}$$

$$\propto \frac{1}{q} \int_{k_F-\Delta k}^{\lambda} kdk \frac{1}{\sqrt{q^2 - 4k^2}},$$

where $\lambda = \min(q/2, k_F)$. So

$$\chi(q) \propto 1, \quad \delta q < 0,$$
$$\chi(q) \propto 1 - [1 - (2k_F/q)^2]^{\frac{1}{2}}, \quad \delta q > 0. \quad (88)$$

The slope of $\chi(q)$ here is everywhere zero or negative, and again we do not obtain a maximum in the susceptibility at Q. So a nesting line does not stabilize the magnetic energy at nonzero Q.

We can use more general bands without undue complication in the case of parallel sheets on the Fermi surface. We again use Equation 84 and orient the coordinates so that the parallel sheets are k_z = constant planes. This time we will expand $E(\underline{k})$ in a Taylor series, take only the first term and use $E(\underline{k}) = E(k_z)$ when we are close enough to the Fermi surface; we also note that $E(k_F) = E(k_F+Q)$. Then we have

$$\chi(q) \propto \int \text{(over points far from the Fermi surface)}$$
$$+ \int_{-L_x}^{L_x} dk_x \int_{-L_y}^{L_y} dk_y \int_{k_F-\Delta k}^{k_F} \frac{dk_z}{E(k_z+q) - E(k_z)}. \qquad (89)$$

$$E(k_z+q) = E(k_F+Q - \delta k_z + \delta q) = E(k_F + Q) - v_1(\delta k_z - \delta q),$$
$$E(k_z) = E(k_F - \delta k_z) = E(k_F) - v_2 \delta k_z, \qquad (90)$$

where v_2 and v_1 are the band velocities at k_F and $k_F + Q$ respectively. So

$$\chi(\delta q) \propto \int_o^{\Delta k} \frac{d(\delta k_z)}{(v_2-v_1)\delta k_z + v_1 \delta q}$$
$$\propto \frac{1}{v_2-v_1} \ln \left| \frac{(v_2-v_1)\Delta k + v_1 \delta q}{v_1 \delta q} \right|. \qquad (91)$$

In this case we see that $\chi(q)$ goes logarithmically to $+\infty$ at Q. Nesting of areas of the Fermi surface is what is required to stabilize the magnetic energy at some nonzero Q, so we can look for parallel sheets of Fermi surface which are nearly k_z = constant planes to identify the peaks we observe in our calculated susceptibility. This connection to the Fermi surface can also serve as a guide to help in the elimination of extraneous peaks introduced by the numerical procedures.

The above calculations for the three different local Fermi surface geometries are very similar to doing the complete calcculation of the susceptibility analytically in the case of three-, two-, and one-dimensional perfectly free-electron bands. The results of this calculation are shown in Figure 6. (Kasuya 1966 is a good reference for more details on the

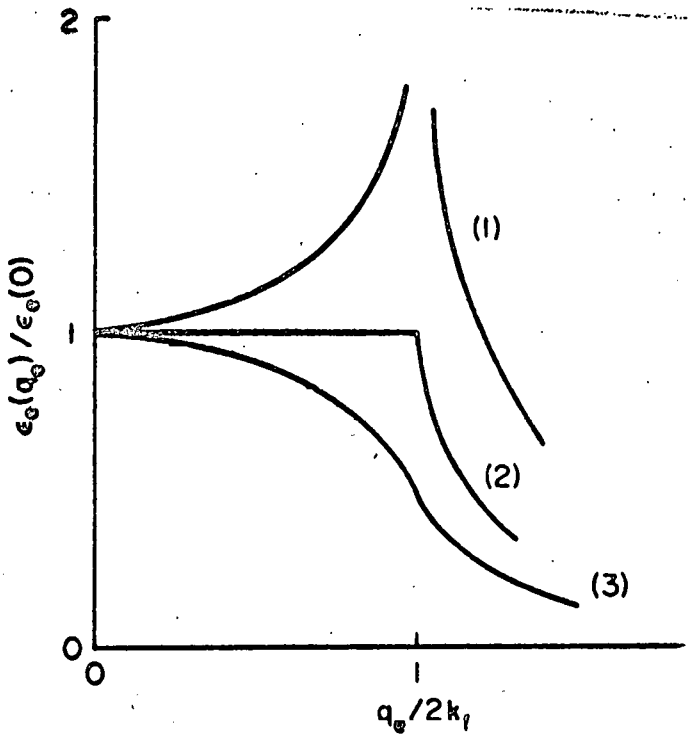

Figure 6. Generalized susceptibilities for completely free-electron energy bands in (1) one dimension, (2) two dimensions, and (3) three dimensions. These correspond to planar, cylindrical, and spherical Fermi surfaces

free-electron susceptibilities, although the calculations are straightforward from the above work.)

In order to allow comparison of the features of the susceptibilities with the Fermi surface geometries, we have prepared a computer program which determines the intersections of the Fermi surface with each of the fifty-eight planes in our interpolated mesh in the double zone. We have intersections of the Fermi surface with the symmetry planes of the zone plotted so we can correlate these with the peaks in the calculated susceptibilities. Results for these Fermi surface plots will be presented in the next chapter along with the susceptibilities. One advantage of this type of procedure is that we can change the Fermi energy and see its effect on both the susceptibility and on the Fermi surface by simply changing the Fermi energy read into the appropriate programs. We will also discuss the effect of varying the Fermi energies in the next chapter.

Cubic and Spherical Fermi Surfaces

We have alluded to the results for the cubic and spherical Fermi surfaces in the above discussion. We will present here the analytical and the numerical calculations for these two geometries assuming a simple cubic lattice of side a, taking $\underline{q} = (0,0,q)$ in the first zone, and considering only the band that determines the Fermi surface, so when we go out of the

zone we make use of a reciprocal lattice vector $\underline{K}_o$ to come back to the same bands.

The cubic Fermi surface may be obtained from the following set of bands:

$$E(\underline{k}) = |k_i| , \tag{92}$$

where k_i means the largest component of $\underline{k}$ in absolute magnitude, and in a simple cubic lattice we require $-\pi/a \leq k_i \leq \pi/a$. To properly put everything in the first zone, we will assume $k_F < \pi/(3a)$, where the cubic Fermi surface has side $2k_F$. Then from Equation 78:

$$\chi(q) = \frac{\Omega}{4\pi^3 N} \int d\underline{k} \, \frac{f_{\underline{k}}(1-f_{\underline{k}+\underline{q}+\underline{K}_o})}{E(\underline{k}+\underline{q}+\underline{K}_o) - E(\underline{k})} . \tag{93}$$

We will break $\chi(q)$ into three parts:

$$\chi(q) = \frac{\Omega}{4\pi^3 N} [(1) + (2) + (3)], \tag{94}$$

where (1) is the part with $k_i = k_z$, (2) has both k_i and $(\underline{k}+\underline{q}+\underline{K}_o)_i = k_x$ or k_y, and (3) has $k_i = k_x$ or k_y and $(\underline{k}+\underline{q}+\underline{K}_o)_i = k_z+q$. In (2) we consider the low temperature limit as the Fermi surface becomes perfectly sharp, which will give density of states terms like those referred to earlier in this chapter that must be added to the numerical calculation. (1) and (3) are rather complicated, but (2), which we need to add to the numerical calculation, is simply

$$\begin{aligned} (2) \quad &= 8k_F^2 - 4k_F q, && 0 < q < 2k_F, \\ &= 0, && q > 2k_F. \end{aligned} \tag{95}$$

We obtain for a final result

$$\chi(q) = \frac{\Omega}{4\pi^3 N}\left[-\frac{2}{3}q^2 + 12k_F^2\right], \qquad 0 < q < k_F,$$

$$= \frac{\Omega}{4\pi^3 N}\left[\frac{4k_F^3}{3q} + 17k_F^2 - 7k_F q + (4k_F^2 - \tfrac{1}{2}q^2)\ln\left(\frac{q}{2k_F - q}\right)\right],$$

$$k_F < q < 2k_F,$$

$$= \frac{\Omega}{4\pi^3 N}\left[\frac{4k_F^3}{3q} + k_F^2 + k_F q + (4k_F^2 - \tfrac{1}{2}q^2)\ln\left(\frac{q}{q - 2k_F}\right)\right], \qquad (96)$$

$$2k_F < q < \frac{\pi}{a} - k_F,$$

$$= \frac{\Omega}{4\pi^3 N}\left[\frac{4}{3q}\left(\frac{\pi}{a}\right)^3 + 5\left(\frac{\pi}{a}\right)^2 - 6k_F\frac{\pi}{a} - 2k_F^2 - 7q\frac{\pi}{a} + \frac{2}{3}q^2\right.$$

$$- \tfrac{1}{2}q^2\ln\left(\frac{q}{q-2k_F}\right) + \left(2\left(\frac{\pi}{a}\right)^2 + 2q\frac{\pi}{a} - \tfrac{1}{2}q^2\right)\ln\left(\frac{q}{\frac{2\pi}{a} - 2k_F - q}\right)$$

$$+ 4\left(\frac{\pi}{a}\right)^2\ln\left(\frac{q}{\frac{\pi}{a} - k_F}\right) + \left(8k_F^2 - 4\left(\frac{\pi}{a}\right)^2\right)\ln\left(\frac{\frac{\pi}{a} - k_F}{\frac{2\pi}{a} - 2k_F - q}\right)$$

$$\left. - 4k_F^2\ln\left(\frac{q - 2k_F}{\frac{2\pi}{a} - 2k_F - q}\right)\right], \quad \frac{\pi}{a} - k_F < q < \frac{\pi}{a}.$$

The contributions (1), (2), and (3) are plotted in Figure 7, where we have taken a = π Bohr radii and E_F = 0.200 Rydberg. In Figure 8 we show the total $\chi(q)$ along with the numerical calculation (with contribution (2) added to the numerical calculation) using the two different meshes that we referred to earlier, each with forty-five points per level for the levels of Figure 5.

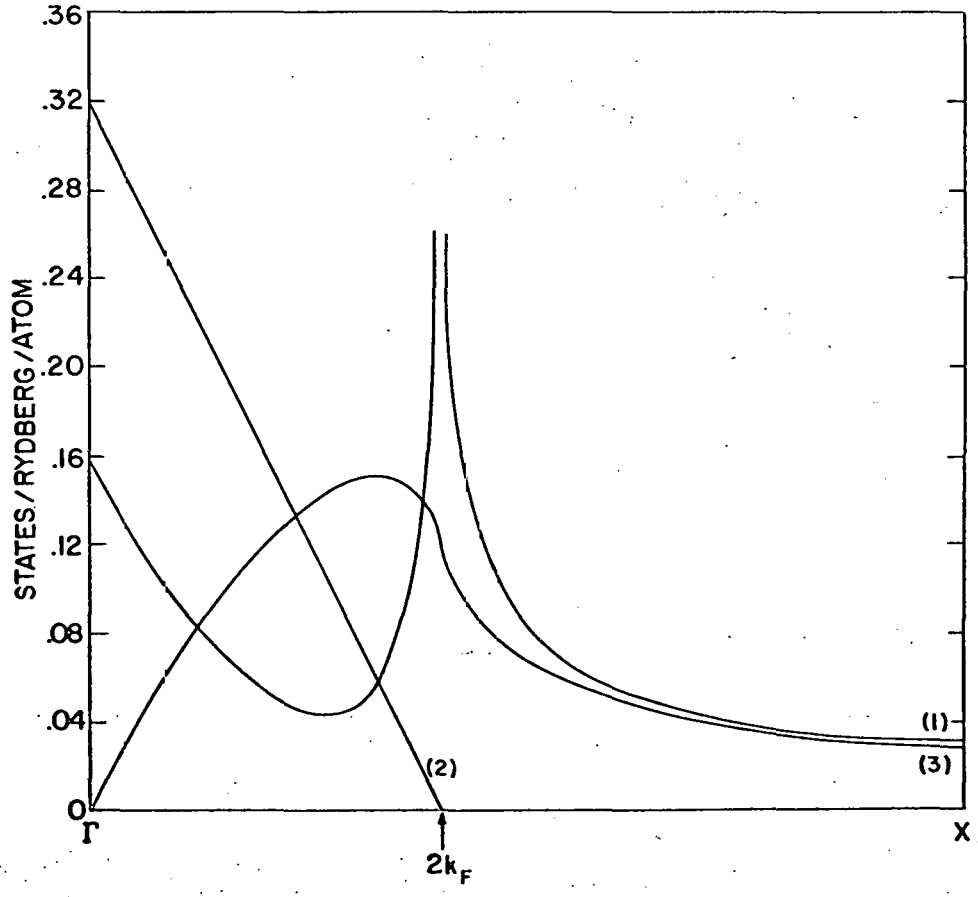

Figure 7. Contributions to the susceptibility for linear bands and cubic Fermi surface

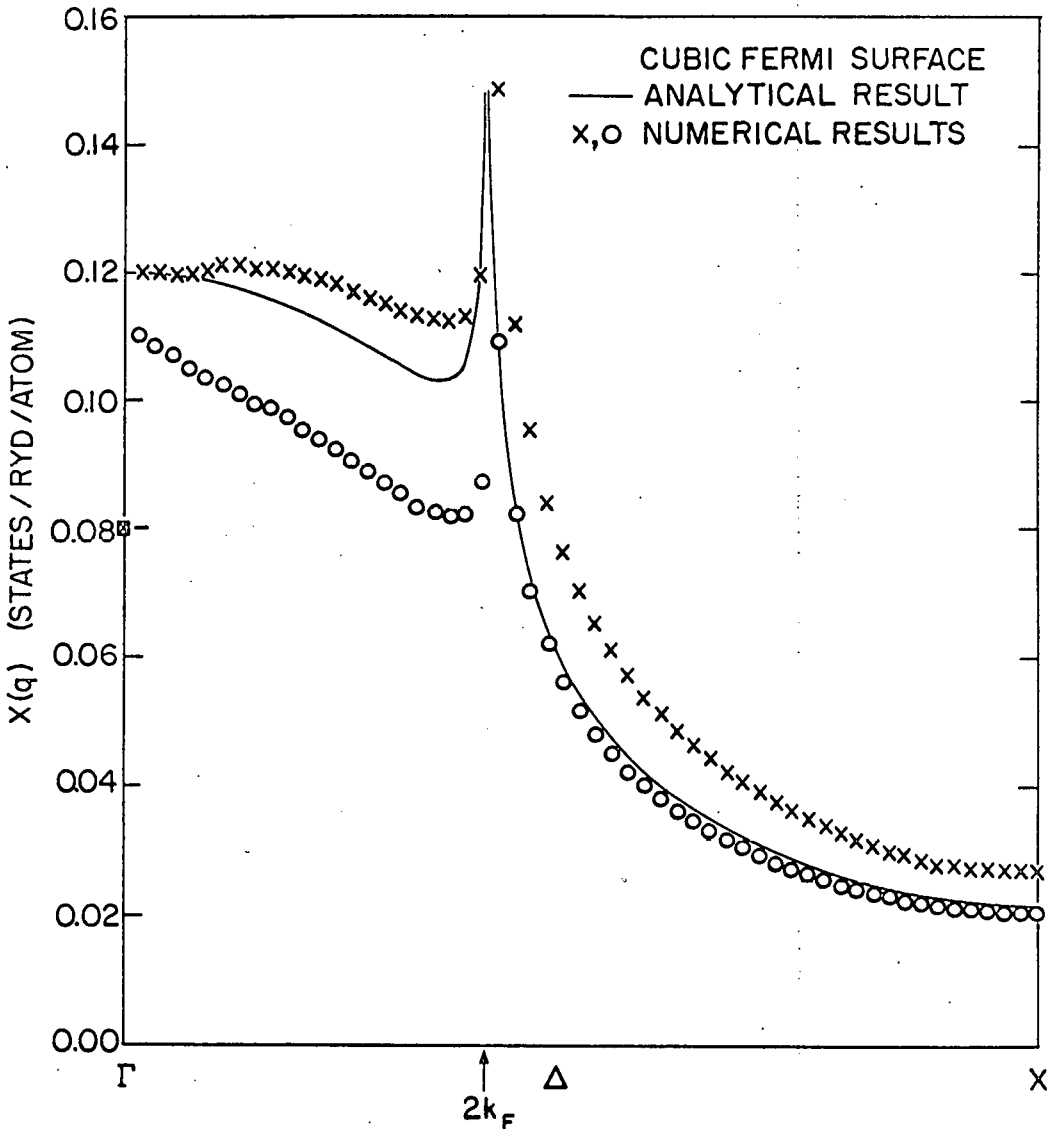

Figure 8. Generalized susceptibility for linear bands and cubic Fermi surface. The solid line is the analytical result. The points are the numerical results for two different meshes

The spherical Fermi surface may be obtained from free-electron bands:

$$E(\underline{k}) = \alpha k^2, \tag{97}$$

where $\underline{k}$ is restricted to a cubic zone of side $2\pi/a$. We will assume that $k_F < \pi/(2a)$, where $2k_F$ is the diameter of the Fermi surface. Then we use the following form for $\chi(q)$:

$$\chi(q) = \frac{\Omega}{4\pi^3 N} \int d\underline{k} \, \frac{f_{\underline{k}}}{E(\underline{k}+\underline{q}+\underline{K}_o) - E(\underline{k})}. \tag{98}$$

Performing the integrations just as in Equations 84 to 86, but for the whole of occupied $\underline{k}$-space this time, we obtain

$$\chi(q) = \frac{\Omega}{8\pi^2 N\alpha} \left[k_F + \left(\frac{k_F^2}{q} - \frac{q}{4}\right) \ln\left|\frac{q+2k_F}{q-2k_F}\right|\right], \quad 0 < q < \frac{\pi}{a} - k_F,$$

$$= \frac{\Omega}{8\pi^2 N\alpha} \left[\left(\frac{q}{4} - \frac{k_F^2}{q}\right) \ln\left|\frac{q-2k_F}{\lambda}\right| + \left(\frac{\lambda}{4} - \frac{k_F^2}{\lambda}\right) \ln\left|\frac{\lambda-2k_F}{q}\right|\right. \tag{99}$$

$$\left. + \frac{k_F}{\lambda}(\lambda - k_F) + \frac{k_F^2}{q\lambda}\left(\frac{\pi}{a} + q\right) - \frac{\left(\frac{\pi}{a}\right)}{q\lambda}\left(\frac{\pi}{a} - q\right)^2\right],$$

$$\frac{\pi}{a} - k_F < q < \frac{\pi}{a},$$

where $\lambda = \frac{2\pi}{a} - q$. We have plotted $\chi(q)$ for $\alpha = 3$, $a = 2\pi$ Bohr radii, and $E_F = 0.066$ Rydberg in Figure 9 along with two numerical calculations for the same two meshes as for the cubic Fermi surface.

We can see that spurious peaks occur in the calculations for the spherical Fermi surface as was mentioned earlier. However, using our criterion that peaks whose positions are

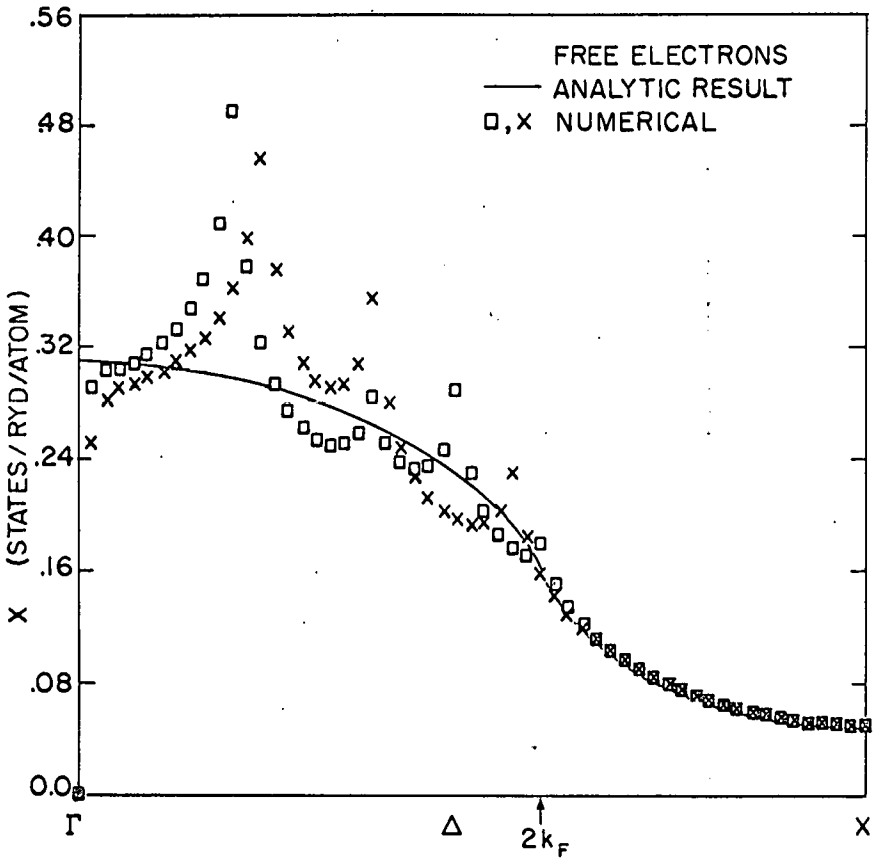

Figure 9. Generalized susceptibility for three-dimensional free electrons. The solid line is the analytical result. The points are the numerical results for two different meshes

mesh-dependent are not real would cause us to eliminate two of the three bad features in this case. If we cared to calculate over still other meshes, the third peak would undoubtedly be removed also, but this is not necessary because we can simply examine the Fermi surface and discover that there are no parallel sheets and therefore eliminate the third peak as arising from the numerical procedures rather than from the energy bands. We notice that the background in both numerical calculations falls quite close to the analytical result, so the simple elimination of the extra peaks as described above will give us a reasonably good picture of the susceptibility.

We have examined the effect of the bands, various meshes, and different Fermi surface geometries in the calculation of the susceptibility in this chapter. The integral for $\chi(q)$ seems to have converged quite well for the mesh we are using; the effect of bands other than those right at the Fermi energy is q-independent, and our knowledge of the Fermi surfaces allows us to eliminate spurious features that may appear in the calculation due to the numerical procedures. When we finally take a look at the calculation for the spherical and the cubic Fermi surfaces, which can also be done analytically, we see that the procedure we have followed seems indeed to be reliable in showing the major features of the susceptibility and, in particular, in predicting the maximum in $\chi(q)$, which interests us because of its relation to stable magnetic ordering arrangements.

THE GENERALIZED SUSCEPTIBILITIES OF THE HEAVY RARE EARTHS

The Calculated Susceptibilities

Following the procedures outlined in the preceeding chapter, we have calculated the generalized susceptibilities of the heavy rare-earth metals: Gd, Dy1, Dy2, Er1, Er2, and Lu, where Dy1, Dy2 and Er1, Er2 correspond to two different potentials used in the band calculations (Keeton and Loucks 1968). The results of these calculations are shown in Figures 10 through 15 in the double-zone representation. In Figures 16 through 21 we show the intersections of the Fermi surface with symmetry planes of the double zone for comparison with the features of the susceptibilities. The dimensions labeled on the Fermi surface sections correspond to the labels on the graphs of $\chi(q)$.

Examination of the Fermi surfaces and comparison with the other calculated susceptibilities indicates that the only real problem with a spurious peak seems to be in Er2, where the first peak in Figure 14 should be eliminated. With the first peak of Er2 removed, there is very little difference between Er1 of Figure 13 and Er2. (There seem to be other spurious peaks in the series of susceptibilities, but they are small enough not to appreciably affect either the shapes of the curves or the analysis of them, so we will not be concerned with them further.) There is also very little difference between the general forms of the susceptibilities of Dy, Er,

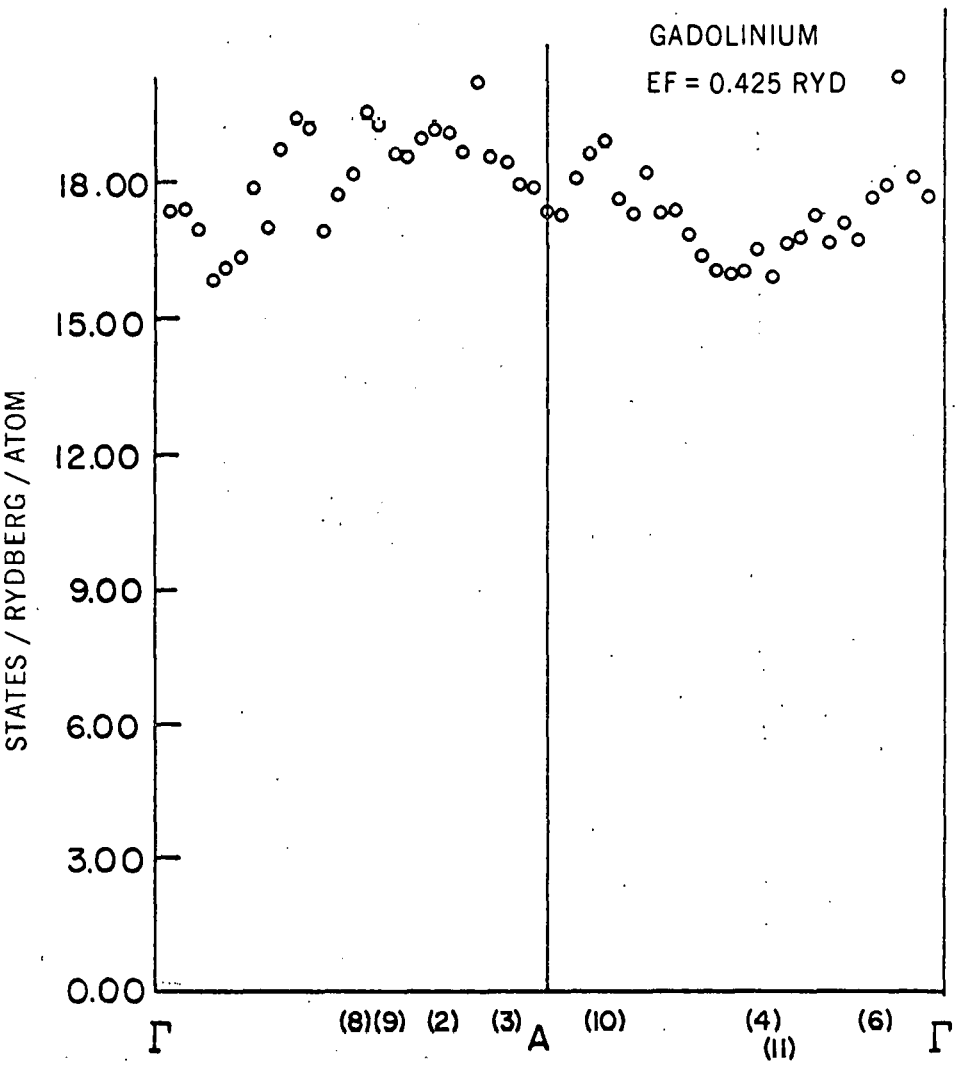

Figure 10. Generalized susceptibility for Gd

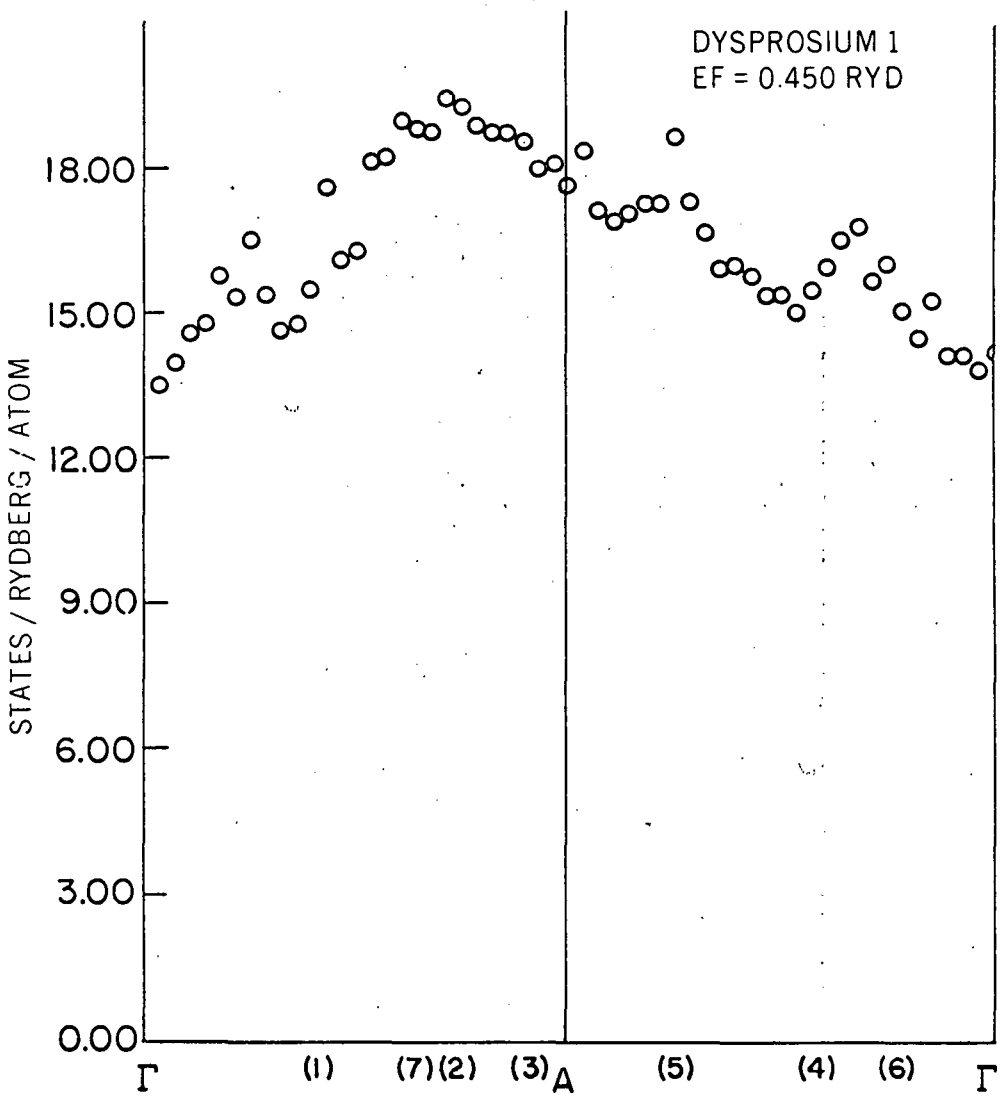

Figure 11. Generalized susceptibility for Dyl

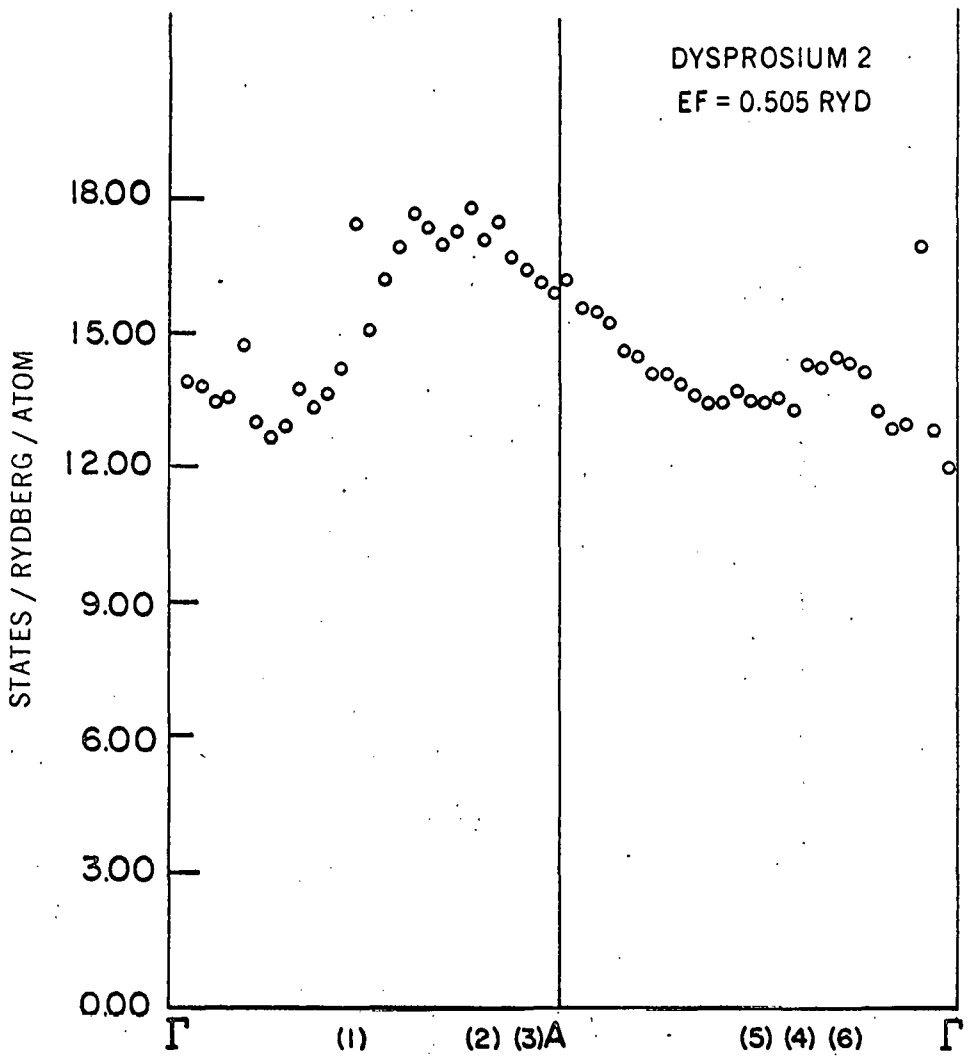

Figure 12. Generalized susceptibility for Dy2

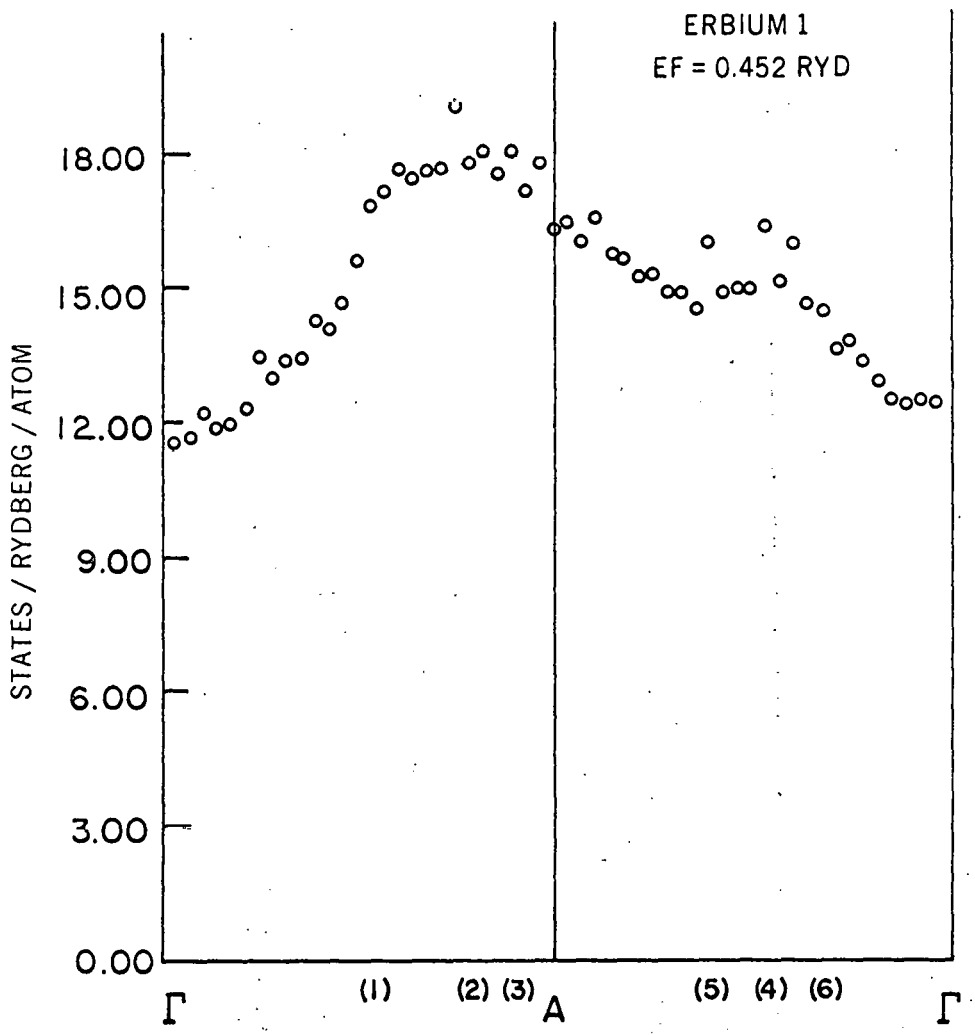

Figure 13. Generalized susceptibility for Erl

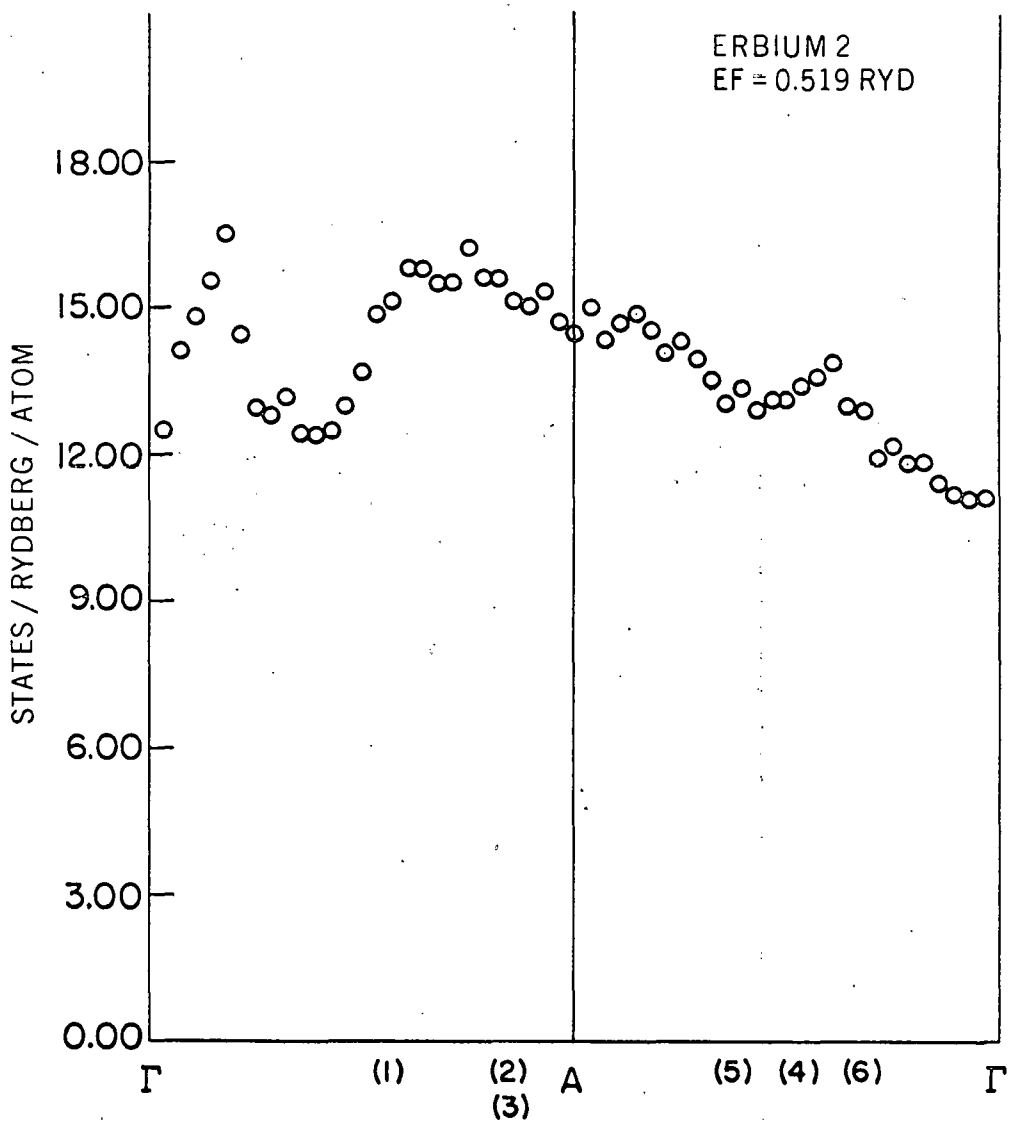

Figure 14. Generalized susceptibility for Er2

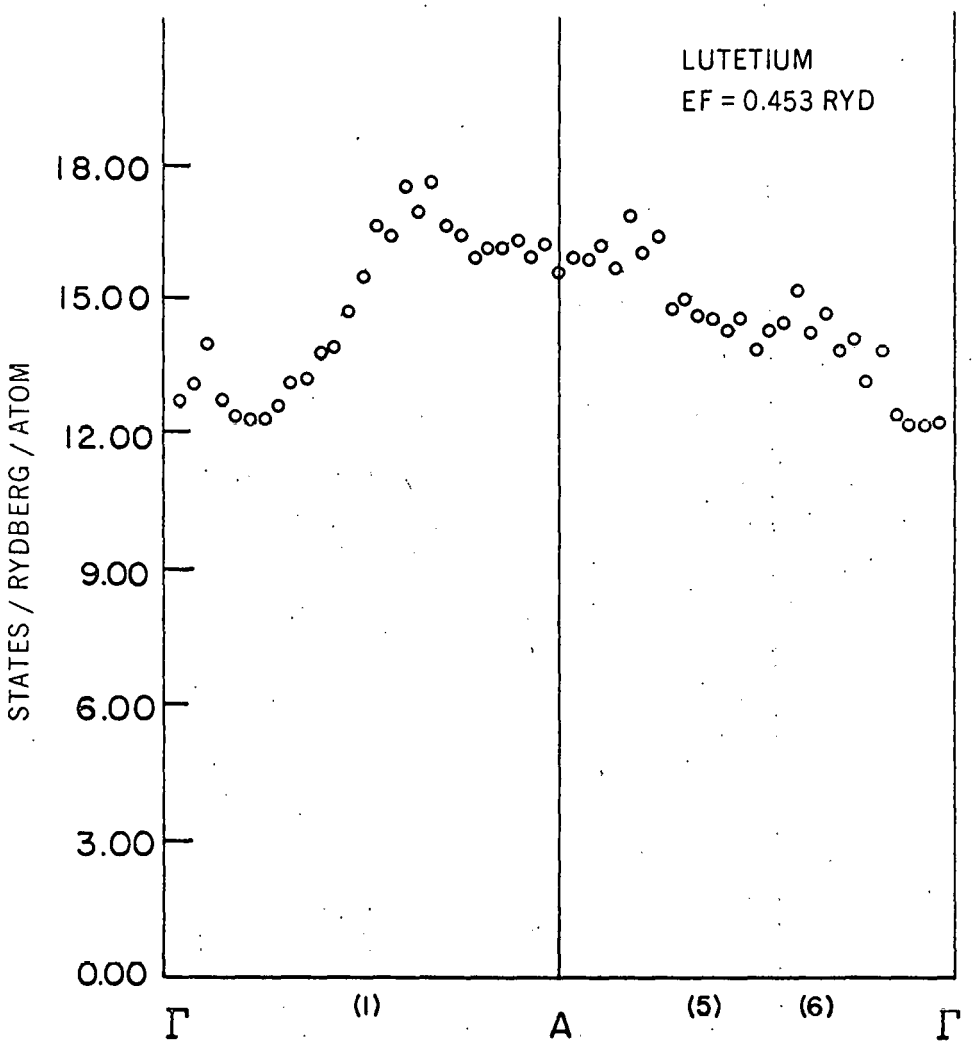

Figure 15. Generalized susceptibility for Lu

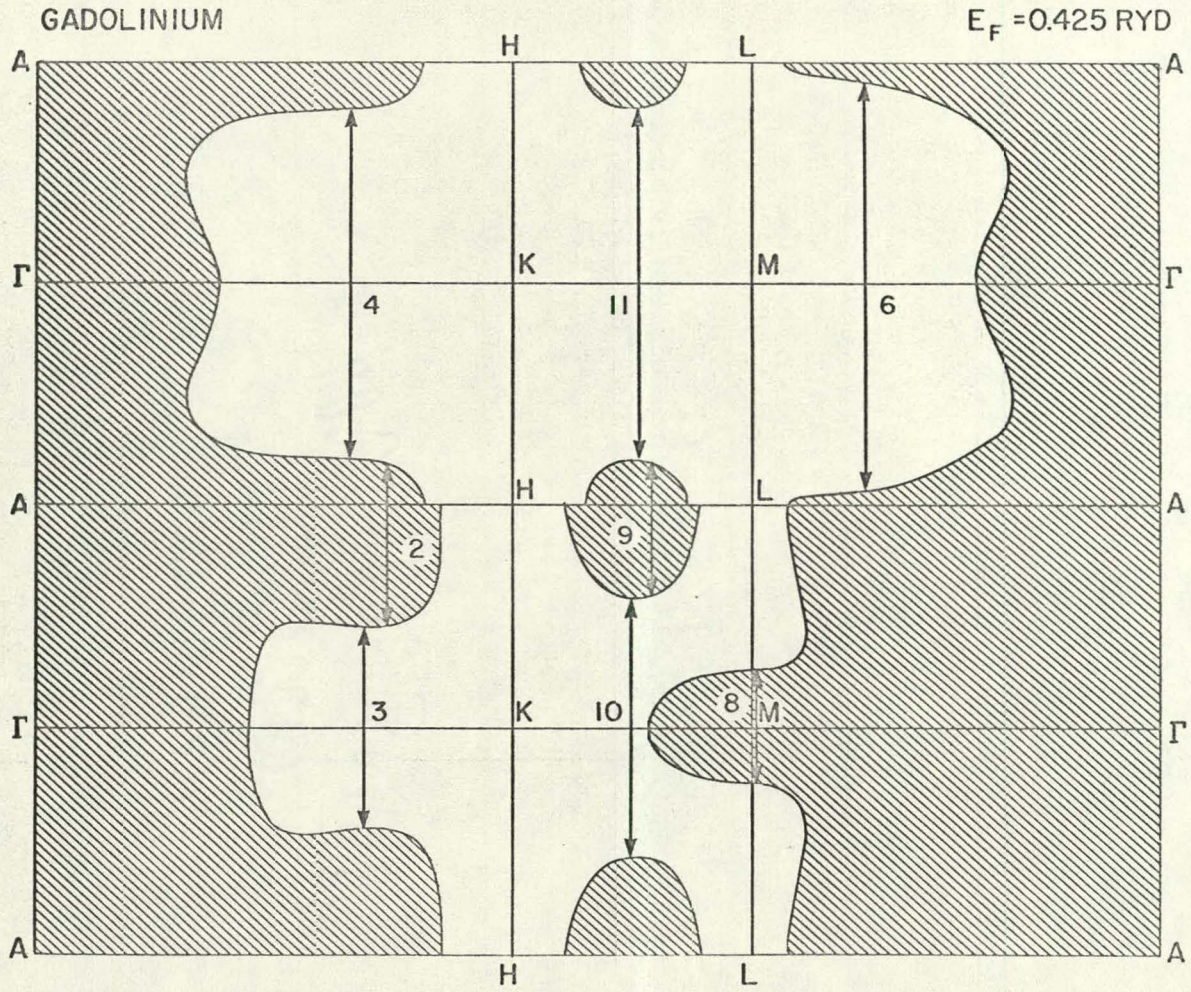

Figure 16. Intersections of the Gd Fermi surface with symmetry planes of the Brillouin zone in the double-zone representation. Crosshatched areas are holes

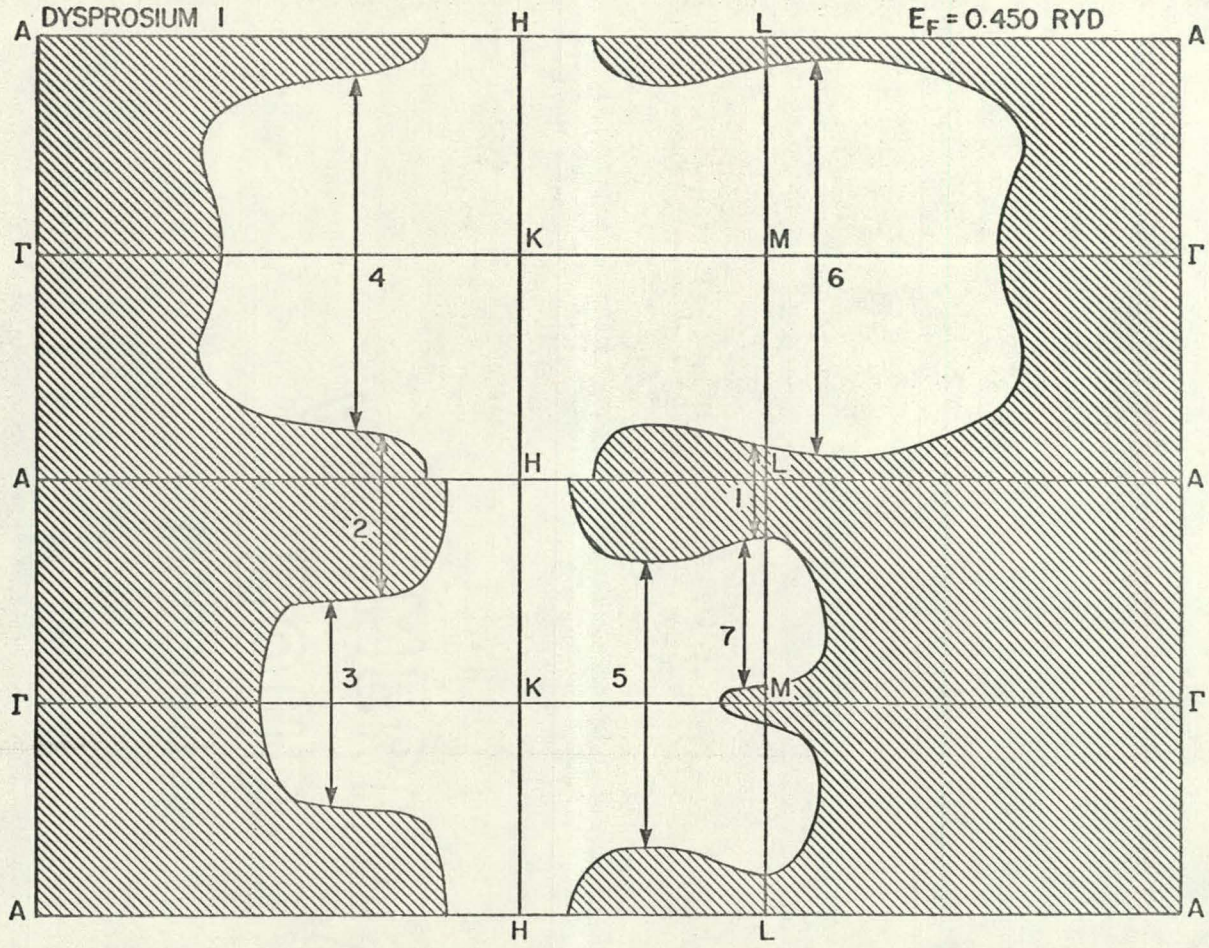

Figure 17. Intersections of the Dyl Fermi surface with symmetry planes of the Brillouin zone in the double-zone representation. Crosshatched areas are holes

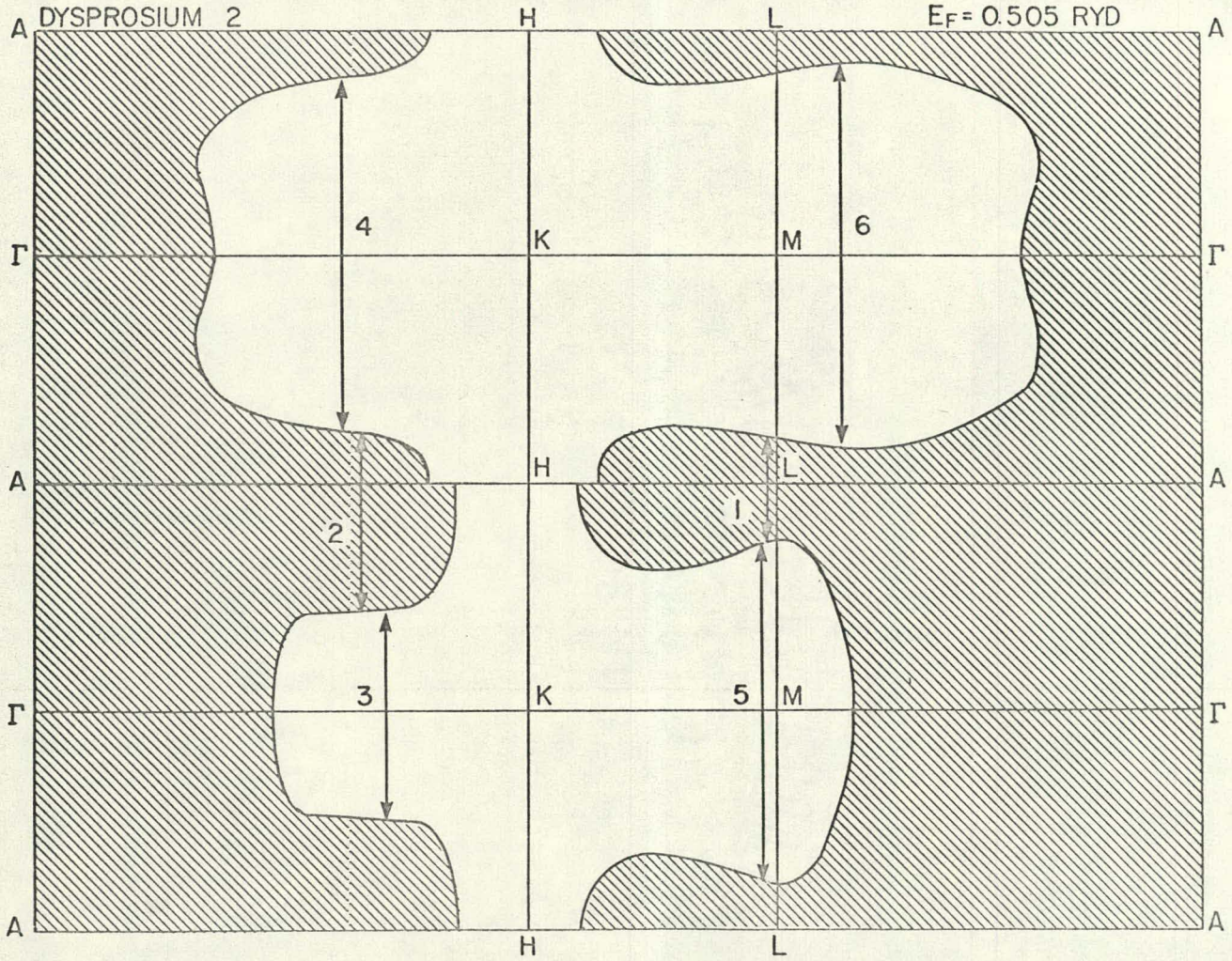

Figure 18. Intersections of the Dy2 Fermi surface with symmetry planes of the Brillouin zone in the double-zone representation. Crosshatched areas are holes

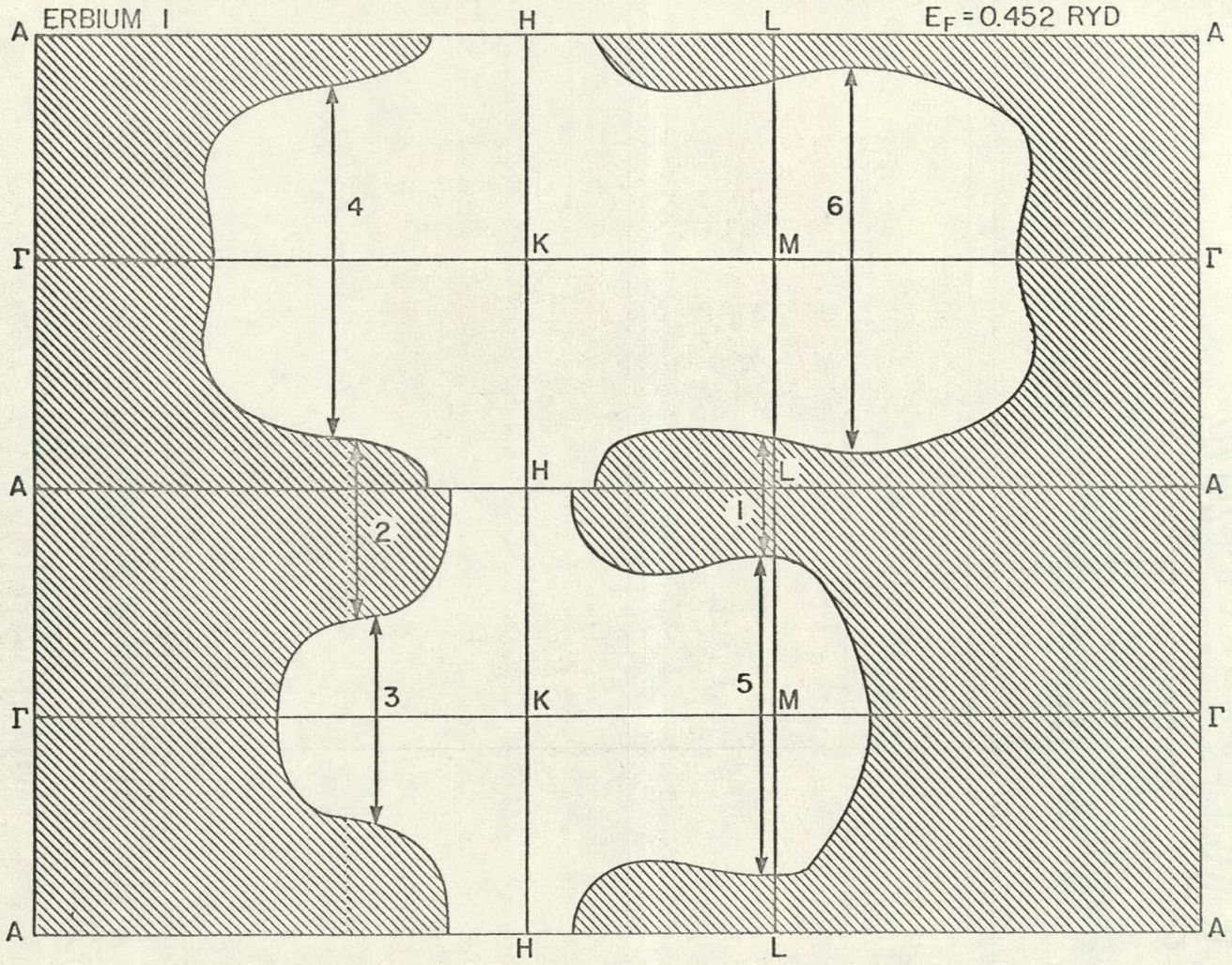

Figure 19. Intersections of the Erl Fermi surface with symmetry planes of the Brillouin zone in the double-zone representation. Crosshatched areas are holes

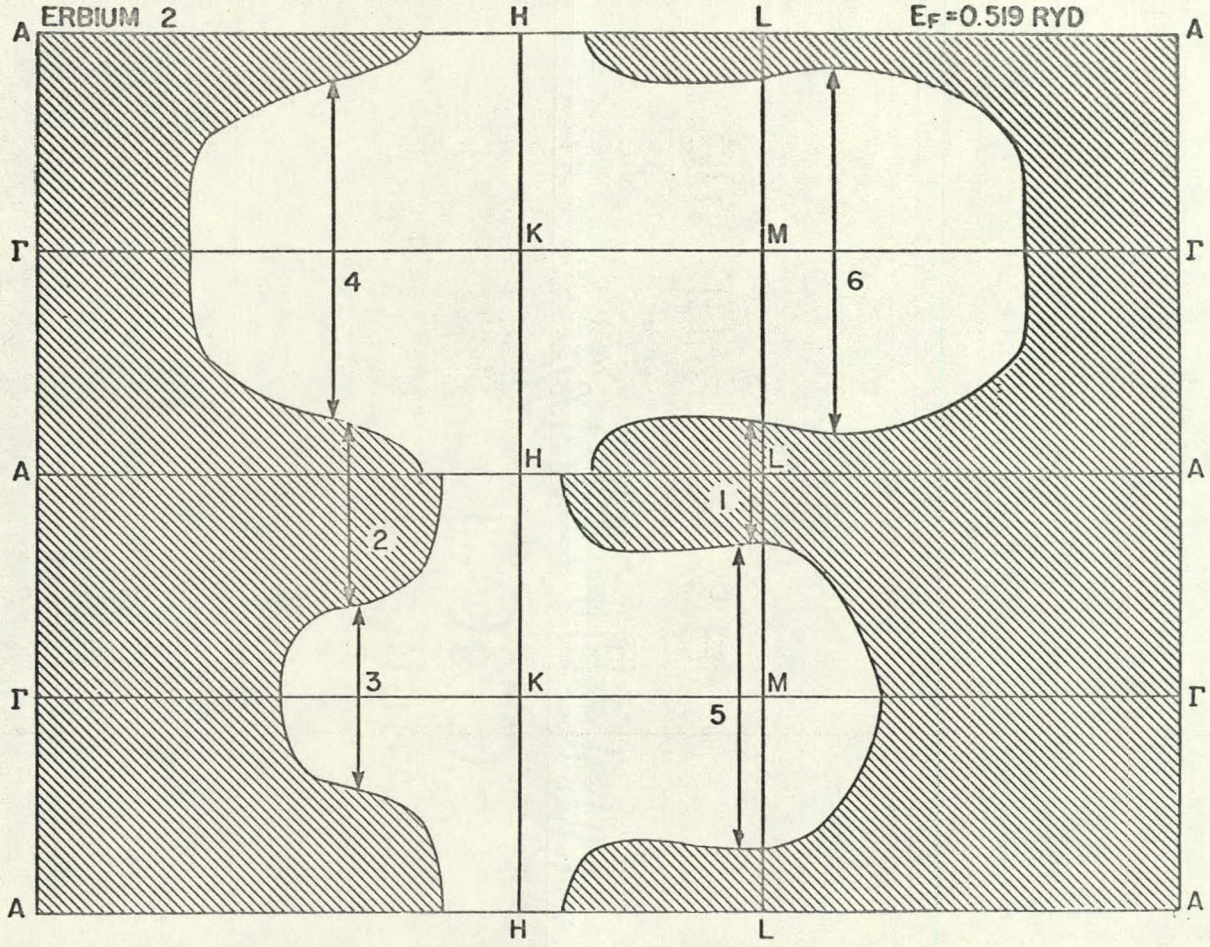

Figure 20. Intersections of the Er2 Fermi surface with symmetry planes of the Brillouin zone in the double-zone representation. Crosshatched areas are holes

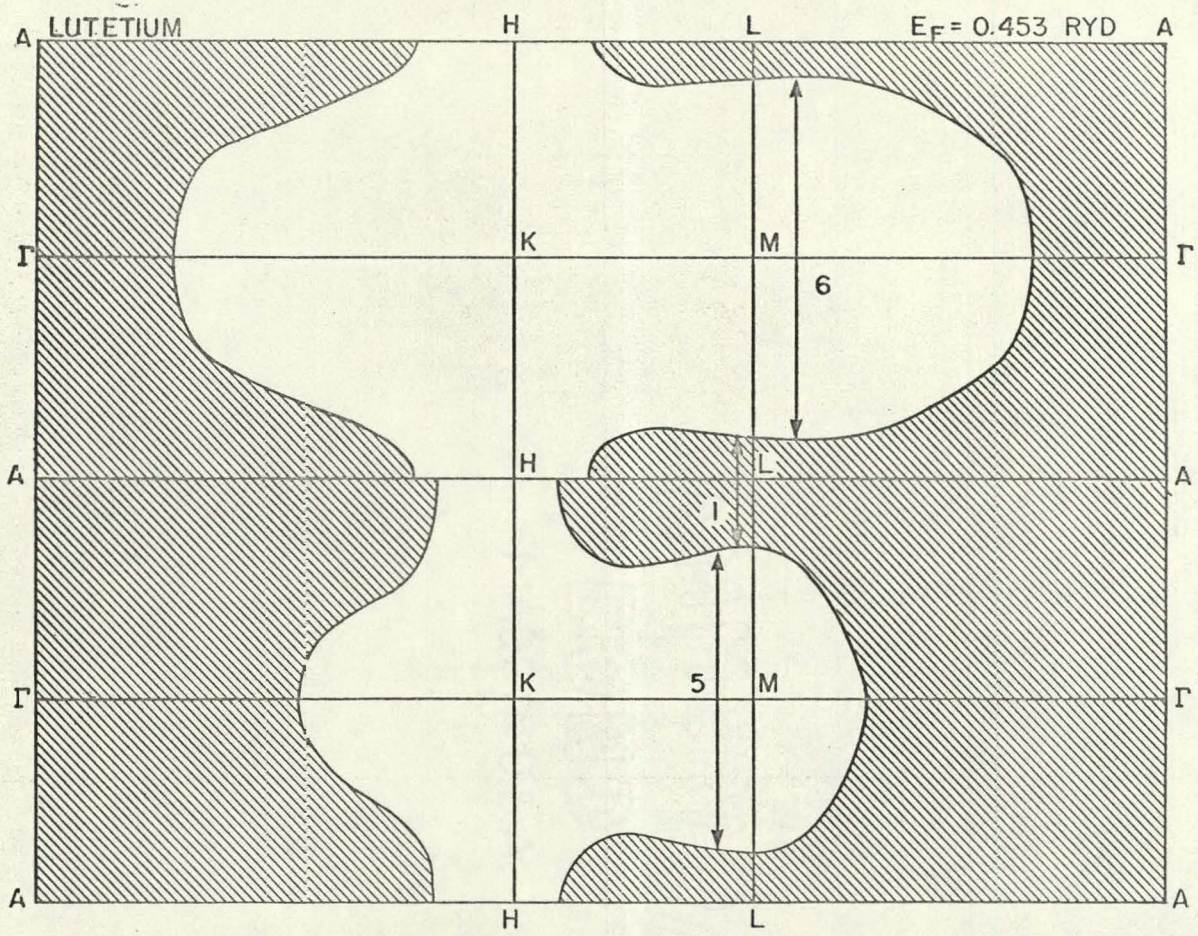

Figure 21. Intersections of the Lu Fermi surface with symmetry planes of the Brillouin zone in the double-zone representation. Crosshatched areas are holes

and Lu, as one might expect by referring back to Table 2 and to Figure 2. This similarity in susceptibilities quite clearly reflects the strong similarity in Fermi surfaces, as seen in Figures 17 through 21.

If we compare the densities of states (times $\frac{1}{2}$) listed in Table 3 with the values of the susceptibilities in Figures 10 through 15 for small q, we see that they are all within a few percent of each other, so that any density of states terms like term (2) in the calculation of the cubic Fermi surface susceptibility must be small enough to be neglected within the accuracy of present bands and the present susceptibility calculation.

Gadolinium is clearly different from the other heavy rare earths in both its Fermi surface and its susceptibility. We shall discuss it separately in some detail in the next section, since it differs from the others in its experimentally determined properties as well as in these theoretical calculations.

We have also calculated both the susceptibilities and the Fermi surfaces for all these metals for Fermi energies .005 Rydberg above and below the Fermi energy calculated by Keeton (1966). The trends are interesting; they seem to be just what one would expect from a simple inspection of the bands. The changes in Fermi surface are such as to make Gd look more like Dy1 when the Fermi energy of Gd is decreased, so with the various Fermi energies we seem to get a set of Fermi surfaces

that make a gradual transition from the gadolinium surface of Figure 16 to the lutetium surface of Figure 21. We will discuss these various surfaces and their susceptibilities more in detail in the following section.

Comparison with Experiment

In Table 2 we have shown some of the magnetic ordering properties of the heavy rare earths including the magnetic wave vector (Q) at the highest ordering temperature for each of the metals in the series. In Table 4 we show the magnetic wave vectors obtained from the maxima in the calculated susceptibilities in comparison with the experimental values. We see that the calculated Q for Lu using the calculated Fermi energy is very close to the experimental Q. Those for Dy and Er are slightly larger than the experimental values, but increasing the Fermi energy by .005 Rydberg improves the agreement considerably. The uncertainties in the bands and in the numerical calculation of the susceptibilities are such that we cannot really expect better quantitative agreement between the experimental and the theoretical Q's than is exhibited for the Q's obtained using the correct Fermi energies. However, the agreement is good enough in each case to give reasonable confidence in the calculation.

When we look at the susceptibilities along side of the Fermi surfaces, with the important nesting q's labeled in both figures, we see that the beginning of the major peak for Dy,

Table 4. Magnetic ordering wave vectors (in units of π/c) as determined from experiment (Koehler 1965) and from the maximum in the theoretical susceptibilities

Metal	Q_{expt}	Q_{theory} (with calculated E_F)	Q_{theory} (with E_F increased by .005 Ryd from calculated E_F)
Dy1	.49	.60	.53
Dy2		.60	.53
Er1	.57	.61	.56
Er2		.61	.54
Lu	.53	.54	.50

Er, and Lu, is in each case determined by the q labeled (1). This has been called the "webbing" q (Kecton and Loucks 1968) because it corresponds to a "webbing" between arms of the Fermi surface. The magnetic Q seems to be greatly influenced by the size of the webbing, and, as we will see in gadolinium, the absence of webbing tends to smear out the features of the susceptibility so that no non-zero Q is selected out from the curve as stabilizing a periodic magnetic structure. The peak in the right half of the susceptibilities of Dy, Er, and Lu seems to come from nesting between pieces of Fermi surface in the same half of the double zone, but the relation of these pieces to the webbing seems to indicate that the webbing also enhances this particular feature of the χ's. Again, comparison with gadolinium seems to bear out this conclusion.

The approximation that all the matrix elements are constants may not be very good. We would expect them to be slightly decreasing functions of q simply because as q increases there should be more and more oscillations in the electron polarization within the 4f-shells of the ions, giving more and more of a tendency for the overlap integrals to cancel out, so that these integrals become smaller as q becomes larger. This should be true even when the sum over reciprocal lattice vectors is carried out, since almost all the terms in such a sum should be smaller for larger q. In a more refined calculation where the q-dependence of the matrix elements could be included, their effect should be to cause the peaks in the calculated susceptibilities to shift slightly to the left as the curve is pulled down, helping to obtain agreement with experiment in Dy, Er, and Lu.

We noted earlier in discussing the kinds of ordering present in the rare earths that Gd has no antiferromagnetic phase but becomes ferromagnetic directly from its paramagnetic phase. This fact would imply that the maximum in the generalized susceptibility of Gd should come at Q = 0. If we examine the form of the susceptibility of Gd in Figure 10, we see that, quite different from the susceptibilities for the other metals, Gd has no apparent peaks but is quite flat across the whole range of q. The effect of a matrix element which is a decreasing function of q would be to pull down the whole curve and

emphasize the stability of the Q = 0 (ferromagnetic) structure. The flatness of the gadolinium susceptibility seems to come from the fact that there are many rather small nesting areas on the Fermi surface (see Figure 16) for a very wide range of q's. This is apparent in Figure 10 as we look at the many important q's which contribute across the susceptibility graph. When the webbing feature is introduced, as in Dy, Er, and Lu, the nesting area for a much smaller range of q's around the webbing q becomes dominant, and we get the peaks which stabilize the periodic magnetic structures in the heavier metals.

We pointed out earlier that the generalized susceptibility is approximately proportional to the magnon spectrum. It can also be shown that the same features of the Fermi surfaces that appear in the magnon spectra and the susceptibilities will appear in the phonon spectra. Therefore, we can look at measured magnon and phonon spectra to see if the same peaks occur in them that we obtain in our theoretical susceptibilities. Experiments have been done on the magnon spectra of Tb (Møller and Houmann 1966), Tb-Ho (Møller et al. 1967 and 1968), and Er (Woods et al. 1967), and on the phonon spectrum of Y (Brun et al. 1968). In each of these cases, bumps (or peaks) are found at Q's equal to the magnetic wave vector for the particular material involved in the study. The experimental existence of these bumps certainly lends support to the shapes we have

calculated for the generalized susceptibilities in the heavy rare earths.

The magnitude of the exchange integral necessary to fit electrical resistivity data is of the order of 0.5 eV (Elliott 1965). If we use a simple effective field approximation we find that

$$kT_c = \frac{I^2 S(S+1)}{3} \chi(Q), \qquad (100)$$

where T_c is the appropriate critical temperature, Q is the magnetic wave vector for the structure at T_c, S = (g-1)J, and I is the exchange integral. We do not know the absolute value of $\chi(Q)$ because we have dropped many q-independent terms, and we only know relative values, like $\chi(Q) - \chi(0)$, under the assumption of constant matrix elements. Therefore, we can look at

$$k(T_N - \theta_P) = \frac{I^2 S(S+1)}{3} [\chi(Q) - \chi(0)] \qquad (101)$$

and compare the magnitude of I with the experimental value to get some idea of how much the q-dependence of the matrix elements must pull down the peaks in $\chi(q)$. Examination of the susceptibilities presented in Figures 11 through 14 gives $\chi(Q) - \chi(0)$ about 6 Rydberg^{-1} for dysprosium and about 4.5 Rydberg^{-1} for erbium. Table 2 gives T_N and θ_P for these metals, and Table 1 gives (g-1)J. When we put these values into Equation 101, we find I about .04 eV for Dy and about .09 eV for Er. This would seem to suggest that the matrix element pulls the peak down so that $[\chi(Q) - \chi(0)]$ is about 10% to 20% of the

value we have calculated or even slightly less. This is probably reasonable since the effective mass of terbium magnons as estimated from the data of Møller and Houmann (1966) seems to be about 1500 electron masses, indicating a reasonably steep increase for the magnon spectrum, and hence a rather steep fall-off for the susceptibility.

When we look at a variety of Fermi energies for the various metals we see that increasing the Fermi energy tends to make the heavier metals look more like Gd and decrease the magnetic Q (this is apparent in Table 4). Decreasing the Fermi energy has the opposite effect, and in fact the Fermi surfaces for Gd with Fermi energy decreased by .005 Rydberg and for Dyl are almost identical. There are, however, some subtle differences between the energy bands for these metals, so that the whole story cannot be told simply by changing Fermi energies for one of the sets of bands.

SUMMARY AND CONCLUSIONS

We have calculated the generalized susceptibilities of the heavy rare earths, Gd, Dy, Er, and Lu, using the energy bands of Keeton and Loucks (1968). This calculation has born out general conclusions drawn previously (Roth et al. 1966 and Keeton and Loucks 1968) about the connection between the Fermi surface geometry and the magnetic wave vector of the periodic magnetic structures observed in these metals. The webbing feature of the Fermi surfaces of Dy, Er, and Lu was pointed out by Keeton and Loucks as being possibly important in the determination of the magnetic wave vector for these materials. Our results have shown, by comparison with the case of Gd where the webbing is not present and by observation of the relation between the size of the magnetic Q and the thickness of the webbing, that the webbing is indeed crucial both in the determination of Q and in the stabilization of the periodic structures observed in these metals.

The energy bands near the Fermi energy as calculated at present seem to give a reasonably consistent picture of the magnetic properties of the heavy rare earths as reflected in our calculated susceptibilities. Quantitative comparison of the susceptibilities with experimental magnon spectra is not at present possible because of our lack of knowledge of the exact form of the q-dependent matrix elements involved in the magnetic energy of these systems and also because of our

incomplete understanding of the effects of anisotropy and magnetoelastic interactions. This type of careful comparison of the calculations with experiment is really necessary before we can say much more about the validity of the energy bands. However, the one piece of experimental information with which there is rather direct comparison is the value of the magnetic Q that should be observed in the periodic structures for these metals. The Q's predicted by our calculation are in quite reasonable agreement with those determined experimentally; this gives confidence in the bands as well as in our generalized susceptibilities.

The existence of bumps in the experimentally measured magnon and phonon spectra (corresponding to the major bumps in our susceptibilities) for these materials adds credence to this theory. It appears that most of the important effects for the determination of the periodic structure for a given metal at its Neel point are contained in the bands and are expressed through the indirect exchange interaction much as we have developed it. The q-dependence of the exchange matrix elements is, of course, still a major obstacle to detailed quantitative comparison of the susceptibilities with the experiments, but the fact that the important features come out of the bands and appear in our calculations indicates that the matrix elements are probably smoothly decreasing functions of q which will not change the conclusions we draw from the susceptibilities.

As we pointed out in the introduction, there are still many approximations involved in the present calculation of the susceptibilities aside from neglecting the q-dependence of the matrix elements which we have discussed in some detail. There is a great deal of theoretical work to be done before all these approximations are fully understood and their effects are taken into account. We are pleased that the improvement we have made through the substitution of realistic energy bands for free-electron bands seems to correspond so well with the experiments in its prediction of the magnetic wave vectors for these metals.

REFERENCES

Brun, T. O., Sinha, S. K., Muhlestein, L. D., and Sakura, J. 1968. Bull. Am. Phys. Soc. 13: 450.

Child, H. R., Koehler, W. C., Wollan, E. O., and Cable, J. W. 1965. Phys. Rev. 138: A1655.

Cohen, Morrel H. and Falicov, L. M. 1960. Phys. Rev. Letters 5: 544.

De Gennes, Pierre-Gilles. 1958. Compt. Rend. 247: 1836.

Elliott, R. J. 1965. Theory of magnetism in the rare earth metals. In Rado, George T. and Suhl, Harry, eds. Magnetism. Vol. 2. Part A. Pp. 385-424. New York, New York, Academic Press, Inc.

Elliott, R. J. and Thorpe, M. F. 1968. J. Appl. Phys. 39: 802.

Herman, Frank and Skillman, Sherwood. 1963. Atomic structure calculations. Englewood Cliffs, New Jersey, Prentice-Hall, Inc.

Herring, Conyers. 1966. Exchange interactions among itinerant electrons. In Rado, George T. and Suhl, Harry, eds. Magnetism. Vol. 4. New York, New York, Academic Press, Inc.

Holstein, T. and Primakoff, H. 1940. Phys. Rev. 58: 1098.

Kaplan, T. A. and Lyons, D. H. 1963. Phys. Rev. 129: 2072.

Kasuya, Tadao. 1956. Progr. Theoret. Phys. (Kyoto) 16: 45.

Kasuya, Tadao. 1966. S-d and s-f interaction and rare earth metals. In Rado, George T. and Suhl, Harry, eds. Magnetism. Vol. 2. Part B. Pp. 215-294. New York, New York, Academic Press, Inc.

Keeton, Stewart C. 1966. Relativistic energy bands and Fermi surfaces for some heavy elements. Unpublished Ph.D. thesis. Ames, Iowa, Library, Iowa State University of Science and Technology.

Keeton, Stewart C. and Loucks, T. L. 1968. [Electronic structure of rare-earth metals. I. Relativistic augmented-plane-wave calculations. To be published in Phys. Rev.]

Kittel, C. 1963. Quantum theory of solids. New York, New York, John Wiley and Sons, Inc.

Koehler, W. C. 1965. J. Appl. Phys. 36: 1078.

Kubo, Ryogo. 1957. J. Phys. Soc. Japan 12: 570.

Liu, S. H. 1961a. Phys. Rev. 121: 451.

Liu, S. H. 1961b. Phys. Rev. 123: 470.

Lomer, W. M. 1962. Proc. Phys. Soc. 80: 489.

Mattis, Daniel C. 1965. The theory of magnetism. New York, New York, Harper and Row, Inc.

Messiah, Albert. 1961. Quantum mechanics. New York, New York, John Wiley and Sons, Inc.

Møller, H. Bjerrum and Houmann, J. C. Gylden. 1966. Phys. Rev. Letters 16: 737.

Møller, H. Bjerrum, Houmann, J. C. Gylden, and Mackintosh, A. R. 1967. Phys. Rev. Letters 19: 312.

Møller, H. Bjerrum, Houmann, J. C. Gylden, and Mackintosh, A. R. 1968. J. Appl. Phys. 39: 807.

Mott, N. F. and Jones, H. 1958. The theory of metals and alloys. New York, New York, Dover Publications, Inc.

Pennington, Ralph H. 1965. Introductory computer methods and numerical analysis. New York, New York, The Macmillan Company.

Roth, Laura M., Zeiger, H. J., and Kaplan, T. A. 1966. Phys. Rev. 149: 519.

Ruderman, M. A. and Kittel, C. 1954. Phys. Rev. 96: 99.

Schwinger, Julian. 1952. On angular momentum. U.S. Atomic Energy Commission Report NYO-3071 [New York Operations Office, AEC].

Specht, Frederick. 1967. Phys. Rev. 162: 389.

Tyablikov, Sergei Vladimirovich. 1967. Methods in the quantum theory of magnetism. New York, New York, Plenum Press.

Villain, J. 1959. J. Phys. Chem. Solids 11: 303.

Watson, R. E., Freeman, A. J., and Dimmock, J. P. 1968. Phys. Rev. 167: 497.

Woods, A. D. B., Holden, T. M., and Powell, B. M. 1967. Phys. Rev. Letters 19: 908.

Yosida, Kei. 1957. Phys. Rev. 106: 893.

ACKNOWLEDGEMENTS

It is a great pleasure to express my sincere appreciation to Dr. S. H. Liu for his active interest and guidance throughout the course of this investigation. I am also very grateful to him for his constant encouragement throughout the course of my graduate study.

I would also like to express my thanks to Dr. C. A. Swenson for the encouragement and counsel that he has given me during my graduate study. I wish to thank Dr. T. L. Loucks for innumerable valuable discussions; his continued interest in this work has been of great help.

I would like to thank the National Science Foundation and the Danforth Foundation for the financial support given me during my graduate work.

Finally, I wish to thank Dr. D. J. Zaffarano for his kindness to me during my stay in the physics department. The opportunities given me to attend important meetings and to advance rapidly in my research and study program have proven very valuable in the successful completion of this investigation.